National Library of Canada
Acquisitions and Bibliographic Services Branch
395 Wellington Street
Ottawa, Ontario
K1A 0N4

Bibliothèque nationale du Canada
Direction des acquisitions et des services bibliographiques
395, rue Wellington
Ottawa (Ontario)
K1A 0N4

Your file Votre référence

Our file Notre référence

NOTICE

The quality of this microform is heavily dependent upon the quality of the original thesis submitted for microfilming. Every effort has been made to ensure the highest quality of reproduction possible.

If pages are missing, contact the university which granted the degree.

Some pages may have indistinct print especially if the original pages were typed with a poor typewriter ribbon or if the university sent us an inferior photocopy.

AVIS

La qualité de cette microforme dépend grandement de la qualité de la thèse soumise au microfilmage. Nous avons tout fait pour assurer une qualité supérieure de reproduction.

S'il manque des pages, veuillez communiquer avec l'université qui a conféré le grade.

La qualité d'impression de certaines pages peut laisser à désirer, surtout si les pages originales ont été dactylographiées à l'aide d'un ruban usé ou si l'université nous a fait parvenir une photocopie de qualité inférieure.

Canada

Theoretical Study of Two Problems in Polymer Physics

by

Songyan Wu

Thesis
Submitted to the University of Ottawa
in partial fulfilment of the
requirements for the degree of
Master of Science in Physics

Ottawa-Carleton Institute for Physics
University of Ottawa
Ottawa,Canada
August,1994

ISBN 0-612-00560-7

UNIVERSITÉ D'OTTAWA
UNIVERSITY OF OTTAWA

Abstract

1. Static Structure Factor and Shape of Reptating Telehelic Ionomers in Electric Fields: We calculate the static structure factor of reptating block copolymers which have a neutral middle block and charged ends. In the presence of an electric field, these telehelic ionomers reptate randomly in their "tubes" but the latter tend to orient along the field axis. If the two ends have different charges, competition between many length scales occurs. The resulting scattering function shows unusual features that are normally characteristic of highly polydisperse mixtures. (results published in Macromolecules, volume 26, number 8, pages 1905-1913).

2. Reptation, Entropic Trapping, Percolation and Rouse Dynamics of Polymer Chains in "Random" Environments: We report the simulation study of the dynamics of linear polymer chains in two-dimensional periodic arrays of obstacles where a fraction 1-c of obstacles are removed. We find Rouse dynamics when c is small, reptation dynamics when c=1, as well as two other regimes between these two limits. Surprisingly, the diffusion coefficient actually decreases when we start removing obstacles. A study of the sites visited by the polymer molecules indicates that the latter are then entropically trapped in large but isolated voids. When about 60% of the obstacles are removed, the large voids form a percolation path and diffusion is easier when further obstacles are removed. Our results thus predict that the diffusion coefficient can vary in a non-monotonic way with concentration.

Acknowledgments

First of all, I would like to express my sincere appreciation and gratitude to Dr Gary Slater for his constant, patient and excellent guidance throughout the course of this work. In addition I also thank him for putting up with the tortuous task of reading the preliminary drafts of this thesis.

I take this opportunity to thank Pascal Mayer, Guy Drouin, Grant Nixon, Bruno Zimm, Jean Louis Viovy, M. Muthukumar, Michael Rubinstein, Ben Widom and David Hoagland for fruitful discussions (with either myself or my supervisor) regarding Part II of this thesis.

I take this opportunity to thank NSERC and the University of Ottawa for financial support in the form of Research and Tuition Fee Waiver Scholarships.

I would also like to thank Grant Nixon who took time to polish the English writing of this thesis, and all support staff and members of the Department for creating such a stimulating atmosphere.

Finally, I wish to thank my husband for his support and encouragement throughout this project.

Contents

Part I

Static Structure Factor and Shape of Reptating Telehelic Ionomers in Electric Fields

Chapter 1

Introduction

Macromolecular science is experiencing an almost explosive growth due to the immensely important role macromolecular materials and the knowledge of their properties play in modern science and technology. Knowing that the present understanding of these materials is still rather limited, we can easily see the necessity for scientists and engineers of all inclinations to understand macromolecular science and develop it further.

The term macromolecule itself suggests that these are large molecules. Some special macromolecular materials (ionomers or polyelectrolytes) can migrate in neutral gels (or entangled solutions of neutral polymers) under the influence of an applied electric field. Since the resulting electrophoretic velocity is often molecular-size dependent, it can be used to obtain a detailed description of the molecular weight distribution. This technique, which is called gel electrophoresis, is widely used in biology to analyze mixtures of nucleic acids[1] or proteins[2] and was recently shown to be applicable to synthetic polyelectrolytes[3].

When one studies the thermal motion of very long molecular chains in polymer gels, the individual macromolecules are surrounded by other molecules (usually refer to as the matrix) that restrict the lateral movement of the segments. Obviously, the restriction is far from complete; the neighbouring chains may move in a concerted fashion, but this relative freedom does not extend very far. The above situation is modeled by imagining that the macromolecule is confined to a tube within the matrix. The diameter of the tube is much larger than that of the chain. The chain can move along the tube but not laterally; the motion is like that of a snake and is accordingly

called reptation. The shortest path connecting the two ends of the chain with the same topology as the chain itself relative to the matrix is called the primitive path. Since the primitive path at any moment represents the conformation of the chain with the small-scale fluctuations omitted, one will use the term 'primitive chain' to denote the dynamical equivalent of the primitive path.

A simple model of gel electrophoresis, known as the biased reptation model, describes the field-driven migration of large charged polymers as the biased reptation of primitive chains in entanglement tubes that tend to be oriented in the field direction[4,5]. This molecular alignment has indeed been observed by various experimental techniques[6,7].

Quite generally, the electric field has two effects on these charged molecules. Firstly, it drives them towards the opposite-sign electrode at a velocity that is a function of field intensity, molecular size, gel concentration and buffer viscosity. Secondly, because the radius of gyration of the migrating molecules is larger than the entanglement spacing (or pore size), the electric forces and the collisions with the gel fibres deform the molecules substantially[4-7]. The interplay between velocity and molecular shape is often subtle and can be modified by the use of pulsed fields[4-9]. Numerous experimental and theoretical investigations of the relationship between velocity and shape have been published[4-9].

Recently, the radius of gyration of telehelic ionomers (copolymers with charged ends and a neutral middle block) has been calculated using a new theorem on reptation[10]. These calculations showed that even if the total charge of the molecule is very small, which results in a negligible electrophoretic velocity, substantial molecular orientation can be achieved if the charge is located near the ends of the molecule. However, the radius of gyration does not give a detailed description of the shape of the molecule.

One can define three classes of telehelic block ionomers[10,11]: (a) both ends have charges of the same sign; (b) the two ends have charges of opposite signs; (c) only one end is charged. The static structure factor of class (b) molecules has been calculated for the special case where the charges were of equal magnitude and the predicted static structure factor was interpreted in terms of the blob picture of chains under stress[11]. However, this is a special case which is probably difficult to realize experimentally.

Ionomers having a charged middle block and end blocks with different (or no) charges form another group of block ionomers. For example, Lumpkin et al.[12] and Slater[13] have studied the case of DNA-like molecules with reduced charges at the ends. Ulanovsky et al.[14] have studied the case of a DNA molecule which has a large neutral globular protein (streptavidin) attached at one of its ends. These molecules have non-zero electrophoretic velocities because of their large total electric charge. This leads to an extra term in the equation of motion (our eq 15; see ref. 11 for a discussion of this point). The molecules treated in the first part on this thesis (Chapters 1-3) have large uncharged middle blocks and can thus be assumed to have negligible velocities; therefore, the dynamics is due to the brownian motion of the chains in their reptation tubes.

In our work, we calculated the exact static structure factor of a general reptating telehelic ionomer. The result can be applied to all three classes mentioned above, regardless of the sign or magnitude of the charges. Our approach uses the biased reptation model. This model has had some success in describing DNA gel electrophoresis, both in constant and pulsed fields. However, it fails when the electric forces are large enough to force the formation of "hernias", molecular loops that penetrate the walls of the reptation tube (for a good discussion of the model and its limitations, see Viovy and Defontaines[15]). Since the telehelic ionomers considered here have

uncharged middle blocks and small charged end blocks, such non-reptation modes of migration cannot occur and the biased reptation model is expected to provide an excellent description of the dynamics of these molecules.

The analysis of the resulting structure factor reveals interesting details about the average shape of these copolymers in the presence of an electric field. In particular, we find that the molecules are characterized by many length scales (up to six), including up to two different blob sizes. Competition between the various length scales lead to intriguing features. The radii of gyration agree with those recently calculated using a master equation[10].

Chapter 2

Calculation of The Static Structure Factor

2.1 The Reptation Model for Telehelic Ionomers

In the reptation model[16,17], the chain is enclosed in an open-ended tube of contour length L defined by the entanglements surrounding it. The motion of the chain is thus essentially one-dimensional. Tube renewal takes place only from the ends. The Langevin equations for the dynamics of a reptating primitive (or effective) bead-rod chain are given by[17]

$$\boldsymbol{R}_n(t+\Delta t) = \frac{1}{2}\,(1+\eta(t))\,\boldsymbol{R}_{n+1}(t) + \frac{1}{2}\,(1-\eta(t))\,\boldsymbol{R}_{n-1}(t) \qquad (1)$$

where $\mathbf{R}_i(t)$ is the position of the i-th bead (with i = 1, 2, ---, N+1), $\eta(t)$ is a stochastic function which takes the value +1 for a forward jump along the tube axis and -1 for a backward jump, and Δt is the average time required by the chain to move over the average distance a between the entanglements (with $a = < | \mathbf{R}_{i+1}(t) - \mathbf{R}_i(t) | >$). The boundary conditions for eq 1 are

$$\boldsymbol{R}_0(t) = \boldsymbol{R}_1(t) + \boldsymbol{a}_1(t) \qquad (2a)$$

$$\boldsymbol{R}_{N+2}(t) = \boldsymbol{R}_{N+1}(t) + \boldsymbol{a}_N(t) \qquad (2b)$$

The first of these equations means that for a backward jump, bead i = 1 moves to a new position $\mathbf{R}_0(t)$ while creating a new tube section of orientation $\mathbf{a}_1(t)$. The second equation has a similar meaning for forward jumps.

We assume that forward and backward jumps are equally probable. The relevance of this assumption in the presence of an electric field will be discussed in chapter 3. Since the end segments of the chain can be charged, the new tube sections $\mathbf{a}_1(t)$ and $\mathbf{a}_N(t)$ cannot be assumed to be randomly oriented, as is normally the case in reptation theories. Instead, $\mathbf{a}_1(t)$ and $\mathbf{a}_N(t)$ will orient preferentially in the field direction[4]. The probability that the charged end segment $\mathbf{a}_{1,N}(t)$ created at time t makes an angle $\theta(t)$ between θ and $\theta+d\theta$ with the field direction is proportional to the Boltzmann factor

$$g_{1,N}(\theta) = \exp\left(\theta_{1,N}\cos\theta\right) \tag{3}$$

where

$$\theta_{1,N} = \frac{\alpha\, Q_{1,N}\, E\, a}{2\,\kappa_B\, T} \tag{4}$$

Here α is a numerical factor which is unity if the end charges $Q_{1,N}$ are uniformly distributed on the end segments, and $\mathbf{E}$ is the electric field intensity. The average projections of the vectors $\mathbf{a}_{1,N}(t)$ on the field axis are thus given by

$$\langle\cos^n\theta\rangle_{1,N} = \frac{\int_0^{\pi}\sin\theta\, d\theta\, \cos^n\theta\, g_{1,N}(\theta)}{\int_0^{\pi}\sin\theta\, d\theta\, g_{1,N}(\theta)} \tag{5}$$

which leads to

$$\langle \cos\theta \rangle_{1,N} = \coth(\theta_{1,N}) - \frac{1}{\theta_{1,N}} \tag{6a}$$

$$\approx \frac{\theta_{1,N}}{3} - \frac{\theta_{1,N}^3}{45} + \ldots \qquad \textit{for } \theta_{1,N}<1 \tag{6b}$$

$$\langle \cos^2\theta \rangle_{1,N} = 1 + \frac{2}{\theta_{1,N}^2} - \frac{2\coth(\theta_{1,N})}{\theta_{1,N}} \tag{6c}$$

$$\approx \frac{1}{3}\left(1 + \frac{2\theta_{1,N}^2}{15} + \ldots\right) \quad \textit{for } \theta_{1,N}<1 \tag{6d}$$

The dimensionless field intensities $\theta_{1,N}$ and molecular size N=L/a will be used in the rest of this thesis. Note that the fields can be positive, negative or zero. In the latter case, one recovers the normal reptation model where the new tube segments are randomly oriented; we then have $\langle\cos\theta\rangle_0 = 0$ and $\langle\cos^2\theta\rangle_0 = 1/3$.

2.2 The Static Structure Factor

The correlation function $G_{mn}(\mathbf{R},t)$ is defined as the probability that the m-th and the n-th segments of the chain are separated by a distance **R** at time t:

$$G_{mn}(R,t) = < \delta\{ [R_m(t) - R_n(t)] - R \} > \tag{7}$$

where $\delta(x)$ is Dirac's delta-function. The structure factor $S(\mathbf{q},t)$ measured in elastic neutron scattering[22] is defined in terms of the Fourier transform of $G_{mn}(\mathbf{R},t)$:

$$S(q,t) = \frac{1}{N^2} \sum_{mn} F_{mn}(q,t) \tag{8}$$

where $\mathbf{q}$ is the wavevector and

$$F_{mn}(q,t) = \int d^3R \exp(iq.R) G_{mn}(R,t) = <\exp\{iq.[R_m(t) - R_n(t)]\}> \tag{9}$$

The averages <...> are carried out for an ensemble of identical chains. Note that since the reptation model does not contain short length scale details, our description is limited to $qa<1$.

From eqs 1 and 9, the Fourier component $F_{mn}(\mathbf{q},t)$ satisfies the equation of motion[11]

$$F_{mn}(q,t+\Delta t) = \frac{1}{2} F_{m+1,n+1}(q,t) + \frac{1}{2} F_{m-1,n-1}(q,t) \tag{10}$$

With $l=ma$, $l'=na$, and $F(l,l',\mathbf{q},t) \equiv F_{mn}(\mathbf{q},t)$, the continum limit of eq 10 for large N gives the following differential equation:

$$\frac{\partial F(l,l',q,t)}{\partial t} = D_c \left(\frac{\partial}{\partial l} + \frac{\partial}{\partial l'}\right)^2 F(l,l',q,t) \tag{11}$$

where $D_c = a^2/2\Delta t$ is the curvilinear diffusion coefficient of the chain in its tube. The corresponding boundary conditions obtained from eqs 2a, 2b, and 9 are[11]

$$\frac{\partial F(l,l',q,t)}{\partial l'} = \left(\frac{iz_1+x_1}{L}\right) F(l,l',q,t) \qquad at\ l'=0 \tag{12a}$$

$$\frac{\partial F(l,l',q,t)}{\partial l} = \left(\frac{-iz_1+x_1}{L}\right) F(l,l',q,t) \qquad at\ l=0 \tag{12b}$$

$$\frac{\partial F(l,l',q,t)}{\partial l} = \left(\frac{iz_N-x_N}{L}\right) F(l,l',q,t) \qquad at\ l=L \tag{12c}$$

$$\frac{\partial F(l,l',q,t)}{\partial l'} = \left(\frac{-iz_N-x_N}{L}\right) F(l,l',q,t) \qquad at\ l'=L \tag{12d}$$

where, with ψ the angle between **q** and **E**,

$$x_i = \frac{L}{2a} \langle [q.a_i(t)]^2 \rangle$$

$$= \frac{1}{2} q^2 La \left\{ \frac{1}{2}\sin^2(\psi) + \left(\cos^2(\psi) - \frac{1}{2}\sin^2(\psi)\right) \langle \cos^2\theta \rangle_i \right\} \tag{13a}$$

$$z_i = \frac{L \langle q.a_i(t) \rangle}{a} = L\, q\, \cos(\psi)\, \langle \cos\theta \rangle_i \tag{13b}$$

To solve eqs 11 and 12, we use the variables[11]

$$s = \frac{l + l'}{L}; \qquad p = \frac{l - l'}{L} \tag{14}$$

Equations 11 and 12 then become

$$\frac{\partial F(s,p,q,t)}{\partial t} = \frac{4D_c}{L^2} \frac{\partial^2 F(s,p,q,t)}{\partial s^2} \tag{15}$$

$$(\frac{\partial}{\partial s} - \frac{\partial}{\partial p})\ F(s,p,q,t) = (iz_1 + x_1)\ F(s,p,q,t) \qquad at\ s = p \tag{16a}$$

$$(\frac{\partial}{\partial s} + \frac{\partial}{\partial p})\ F(s,p,q,t) = (-iz_1 + x_1)\ F(s,p,q,t) \qquad at\ s = -p \tag{16b}$$

$$(\frac{\partial}{\partial s} + \frac{\partial}{\partial p})\ F(s,p,q,t) = (iz_N - x_N)\ F(s,p,q,t) \qquad at\ s = 2-p \tag{16c}$$

$$(\frac{\partial}{\partial s} - \frac{\partial}{\partial p})\ F(s,p,q,t) = (-iz_N - x_N)\ F(s,p,q,t) \qquad at\ s = 2+p \tag{16d}$$

The boundary conditions 16a and 16c are for p>0, while 16b and 16d are for p<0. Finally, the static structure factor S(q,t), in terms of the relative variables s and p, is given by

$$S(q,t) = \frac{1}{2} \int_0^1 ds \int_{-s}^{s} dp\ F(s,p,q,t) + \frac{1}{2} \int_1^2 ds \int_{s-2}^{2-s} dp\ F(s,p,q,t) \tag{17}$$

In the steady state, i.e. for $t \to \infty$, we have $\partial F/\partial t = 0$, and the solution of eq 15 is

$$F_\infty(s,p,q) = A(p)\ s + C(p) \tag{18}$$

where the "constants" of integration A(p) and C(p) are to be found from the conditions 16. We will not study the time dependence of S(q,t) in this thesis.

2.3 The Zero-Field Case

As a useful example, we derive here the static structure factor for the equilibrium (zero-field) case. According to eqs 6 and 13, we have, for $\mathbf{E} = 0$,

$$z_1 = z_N = 0 \tag{19a}$$

$$x_1 = x_N \equiv x^{(0)} = q^2 \frac{La}{6} = q^2 R_g^2 \tag{19b}$$

where $R_g=(La/6)^{1/2}$ is the radius of gyration of the chain in equilibrium[25]. The solution of eqs 15 and 16 is then

$$F_{equ}(s,p,q) = \exp\left(-q^2 R_g^2 |p| \right) \tag{20}$$

from which eq 17 gives

$$S_{equ} = D(q^2 R_g^2) \tag{21a}$$

$$\approx 1 - \frac{1}{3} q^2 R_g^2 + \ldots \qquad for\ qR_g \ll 1 \tag{21b}$$

$$\approx \frac{2}{q^2 R_g^2} + \ldots \qquad for\ qR_g \gg 1 \tag{21c}$$

where $D(x) = 2(x - 1 + e^{-x})/x^2$ is the Debye function. These well-known results[25] indicate that

$S_{equ}(\mathbf{q})$ measures the average dimensions of the equilibrium chain.

2.4. The Static Structure Factor in the General Case

We now derive the static structure factor for the general case. With the scattering factors $z_{1,N}$ and $x_{1,N}$, we can solve eqs 16a and 16c for A(p) and C(p), as defined by eq 18, to obtain

$$A(p) = K_1 e^{-(x_1+iz_1)p} + K_2 e^{-(x_N-iz_N)p} \tag{22}$$

$$C(p) = \frac{1}{iz_1+iz_N+x_1-x_N}[K_1 e^{-(x_1+iz_1)p}(x_1p-x_Np-2x_1+$$

$$2x_N+2+iz_1p+iz_Np-2iz_1-2iz_N)$$

$$+K_2 e^{-(x_N-iz_N)p}(x_Np-iz_Np+2-iz_1p-x_1p)] \tag{23}$$

where the constants $K_{1,2}$ are fixed by the conditions

$$\lim_{p\to 0} F_\infty(s,p,q) = 1 \tag{24a}$$

$$\lim_{z_1\to 0}\lim_{z_N\to 0}\lim_{x_1\to x^{(0)}}\lim_{x_N\to x^{(0)}} F_\infty(s,p,q) = F_{equ}(s,p,q) \tag{24b}$$

We find $K_1=-K_2=-1/2$, from which eqs 18, 22 and 23 give

$$F_\infty(s,p>0,q) = \frac{1}{2}\left[e^{-(x_N-iz_N)p} - e^{-(x_1+iz_1)p} \right] s +$$

$$\frac{1}{2(iz_1+iz_N+x_1-x_N)}\ [\ e^{-(x_N-iz_N)\,p}(-x_1p+x_Np+2-iz_1p-iz_Np)$$

$$-e^{-(x_1+iz_1)\,p}(x_1p-x_Np-2x_1+2x_N+2+iz_1p+iz_Np-2iz_1-2iz_N)] \qquad (25)$$

Similarly, solving eqs 16b, 16d, 24a and 24b for p<0, we get

$$F_\infty(s,p<0,q)\ =\ \frac{1}{2}\ [e^{(\,x_N+iz_N)\,p}\ -\ e^{-(x_1-iz_1)\,p}\ ]\ s+$$

$$\frac{1}{2(-iz_1-iz_N+x_1-x_N)}\ [\ e^{(x_N+iz_N)\,p}(x_1p-x_Np+2-iz_1p-iz_Np)$$

$$-e^{(x_1-iz_1)\,p}(-x_1p+x_Np-2x_1+2x_N+2+iz_1p+iz_Np+2iz_1+2iz_N)] \qquad (26)$$

With eqs 25 and 26, eq 17 gives

$$S_\infty(q)=\Omega(x_1,z_1)+\Omega(x_N,z_N)+\phi(z_1,x_1,z_N,x_N)+\phi(z_N,x_N,z_1,x_1) \qquad (27)$$

Here, $\Omega(x,z)$ and $\Phi(z_i,x_i,z_j,x_j)$ are defined as:

$$\Omega(x,Z)\ =\ \frac{x^5-2x^4+2x^3+2x^3z^2+xz^4-6xz^2+2z^4}{(x^2+z^2)^3}\ -$$

$$\frac{2\ e^{-x}\ [\ (x^3-3xz^2)\ \cos(z)\ +\ (z^3-3x^2z)\ \sin(z)\ ]}{(x^2+z^2)^3} \qquad (28)$$

$$\phi(z_i,x_i,z_j,x_j)=\frac{2(z_i^4-x_i^4+x_i^3x_j+z_i^3z_j+z_i^2x_ix_j+x_i^2z_iz_j+x_i^3-x_i^2x_j+x_jz_i^2-2x_iz_iz_j)}{[\ (x_i-x_j)^2+(z_i+z_j)^2\ ]\ (x_i^2+z_i^2)^2}$$

$$+\{2e^{-x_i}[(x_i^2x_j-x_i^3-z_i^2x_j+3x_iz_i^2+2x_iz_iz_j)\cos(z_i) \tag{28}$$

$$+\ (x_i^2z_j-z_i^2z_j-z_i^3+3x_i^2z_i-2x_iz_iz_j)\sin(z_i)]\}$$

$$/\{[(x_i-x_j)^2+(z_i+z_j)^2](x_i^2+z_i^2)^2\} \tag{29}$$

In the next sections we study the various features predicted to occur on the $S_\infty(\mathbf{q})$ vs q curves using our general solution given by eqs 27-29, the main results of the first part of this thesis. Note that eq 27 reduces to eq 48 of ref. (11) when $Q_1=-Q_N$, as it should be.

2.5 Results

The steady-state static structure factor $S_\infty(\mathbf{q})$ depends entirely on the parameters $x_{1,N}$ and $z_{1,N}$ which come from the four boundary conditions given by eqs 16. As mentioned before, there are four classes of telehelic ionomers, defined according to their boundary conditions $x_{1,N}$ and $z_{1,N}$, i.e., according to their end-segment charges Q_1 and Q_N. Figure 1 shows schematic examples for each of the four classes. In class a, we have $Q_1Q_N<0$, and the end segments point in opposite

directions in an electric field, thus giving the chain an elongated I-shaped conformation. In class b, $Q_1Q_N>0$, and the end segments are pointing in the same direction, giving a typical J-shaped conformation. In class c, one charge is zero while the other is finite; the electric field then affects only the part of the chain for which the reptation tube has been generated by the charged end segment, the rest of the chain staying in a random-walk conformation. Finally, when $Q_1=Q_N=0$, the electric field does not modify the evolution of the tube (class d is thus same as the zero-field case treated in section 2.3 above).

Before we discuss the static structure factor for the three non-trivial classes a-c, we introduce below the length scales involved in the problem, a useful theorem on reptation, and finally the value of the radius of gyration in some special cases.

2.5.1 The Length Scales

There are six important length scales in the problem. The first one is a, the average distance between entanglements. Usually, we take a as a constant fixed by the topology of the problem; in a gel matrix, a would be given by the average pore size. The second one is the wavelength 1/q used to probe the structure; the reptation theory is valid only for qa<1. A third length is the length of the reptation tube L=Na, which is proportional to the contour length of the molecule itself.

The fourth and the fifth length scales are related to the boundary condition parameters $x_{1,N}$ and $z_{1,N}$. The equilibrium conformation ($Q\mathbf{E}=0$) is characterized by the radius of gyration R_g; to first order in E, the ratio between the lengths R_g and q^{-1} defines the parameters x_i. The electric force $Q_i\mathbf{E}$ brings in the anisotropic conformation length ξ_i^{ψ} defined as

$$\xi_i^{\psi} = L \mid \langle \cos\theta \rangle_i \cos(\psi) \mid \qquad (30)$$

This length measures the orientation (at an angle ψ from **E**) of a tube generated by an end segment having an average projection $\langle\cos\theta\rangle$ on the field direction. The ratio between ξ_i^{ψ} and q^{-1} defines the parameter z_i. Of course, $\xi_i^{\perp} = 0$ since the field does not induce order in the transverse plane. Note that if $|Q_1| \neq |Q_N|$, eq 30 defines two lengths ξ_i^{ψ} when both ends of the molecule are charged.

The boundary conditions show a competition between R_g and ξ_i^{ψ} (if at least one end segment is charged) since $z_i^2/x_i \approx (\xi_i^{\psi}/R_g)^2$. At low fields, $R_g > \xi_i^{\psi}$, and x_i leads to almost isotropic random-walk conformations (the dependence of x_i on $\langle\cos^2\theta\rangle_i$ makes it slightly anisotropic). At large fields, however, we have $R_g < \xi_i^{\psi}$ and $R_g > \xi_i^{\perp}$, and the chain conformations are oriented in the field direction (over a length $\sim\xi_i^{I}$), but slightly shrunk in the transverse plane.

For class a chains, strong electric forces lead to an I-shaped conformation (Figure 1a), with an average end-to-end distance of order ξ^{I}. For class b, the chains fold in two (Figure 1b), with both ends pointing in the field direction; the length of the two arms of the J-shaped conformation are then proportional to the lengths ξ_i^{I} (at high fields). In class c, a part of the chain is oriented in the field direction, with an isotropic characteristic length scale ξ_N^{I}, while the rest stays in a quasi-isotropic random-walk conformation with a length scale R_g (see Figure 1c).

The last length scale is the blob size b_i defined by $b_i = R_g^2/\xi_i^{\psi}$. It can be interpreted in the following way: We will see in section 2.5.3 that for $q > 1/b_i$, the static structure factor is the same as for an equilibrium chain. This means that the electric forces are not strong enough to modify

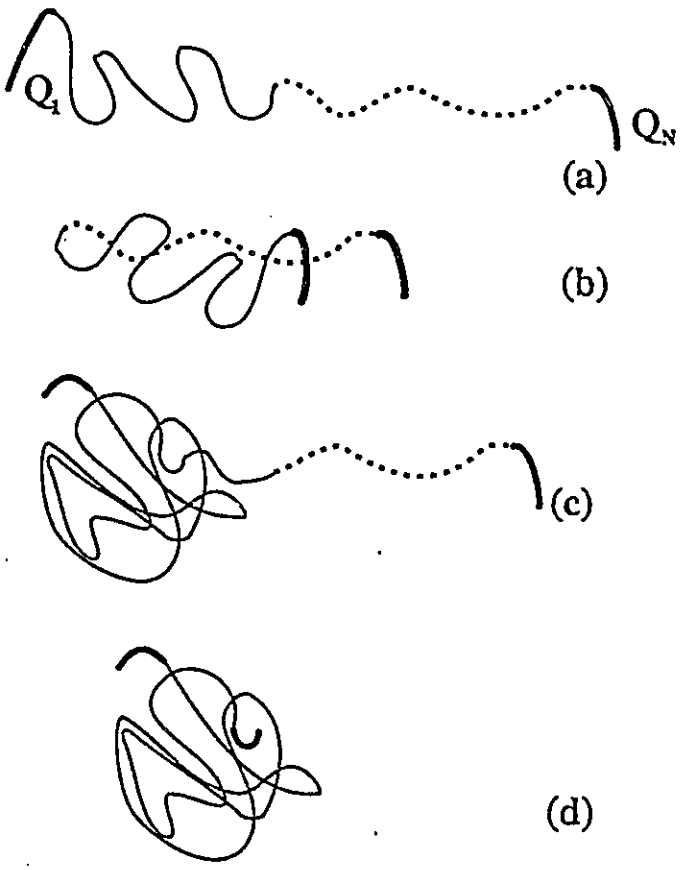

Figure 1. Schematic high-field conformations for the four classes of charged polymer chains. (a) $Q_1Q_N<0$: the end segments points in opposite directions with two anisotropic orientation lengths ξ_1^I and ξ_N^I, and the chain orients to take an I shape. (b) $Q_1Q_N>0$: the end segments point in the same direction with two anisotropic orientation lengths ξ_1^I and ξ_N^I, giving a J shape conformation. (c) Only one end segment is charged: this segment orients a part of the chain with an anisotropic orientation length ξ_N^I, while the rest stays in a (zero-field-like) random-walk conformation. (d) $Q_1=Q_N=0$: the chain has a random-walk conformation. Dashed and solid lines show different degree of orientation; the end segments are thicker. These conformations represent average molecular shapes and orientations, not snapshots.

the random-walk conformation over lengths smaller than b_i. A volume of size b_i^3 contains $n_i=b_i^2/a^2$ segments if these segments stay in a random-walk conformation. We can describe the three kinds of (average) oriented conformations (Figure 1) as series of N/n_i random-walk "blobs" of size b_i aligned by the electric forces (which act effectively over lengths larger then b_i). The dimension of an oriented conformation is therefore proportional to $(N/n_i)b_i=\xi_i^{\nu}$, as expected. Since the field does not align the blobs in the transverse direction, they act as an effective segment of length b_i following a transverse random walk with dimension $(N/n_i)^{1/2}b_i \approx R_g$. Of course, if the charges Q_1 and Q_N are of unequal magnitudes, two different blob sizes b_i and length scales ξ_i^{ν} will compete. This leads to interesting effects, as we will see later.

2.5.2 A Useful Theorem on Reptation

We now briefly review a recent theorem on reptation that will be most useful to interpret our results[10]. In the reptation model, the chain can be represented by a series of N vector segments $\mathbf{r}_i$ with $\mathbf{r}=\mathbf{R}_{i+1}-\mathbf{R}_i$ ($1\le i\le N$), where $\mathbf{r}_1$ and $\mathbf{r}_N$ are thus the end segments of the chain. Since new tube sections are created only when the $\mathbf{r}_1$ and $\mathbf{r}_N$ end segments leave the original tube, all orientations $\mathbf{r}_i$ of the N tube segments have been chosen in the past by the one of the two end segments (we neglect here tube leakage or any other degree of freedom not included in the ideal reptation model). Because the chain is continuous, the n_+ segments that owe their present orientation to past $\mathbf{r}_N \rightarrow \mathbf{a}_N$ jumps are consecutive, starting from the end segment $\mathbf{r}_N$. Similarly, the $n_- = N - n_+$ segments oriented in the past by $\mathbf{r}_1 \rightarrow \mathbf{a}_1$ jumps are consecutive, starting from $\mathbf{r}_1$. If we denote by $g(n_+,t)$ the probability that n_+ segments of the chain owe their orientation at time t to past $\mathbf{r}_N \rightarrow \mathbf{a}_N$ jumps, we have, in the steady-state[10] (i.e. when $\partial g(n_+)/\partial t=0$):

$$g(n_+,t) \equiv g(n_+) = \frac{1}{N+1} \qquad with\ 0 \le n_+ \le N \tag{31}$$

We get a surprising result: In the steady state, all tube segments (including $\mathbf{r}_1$ and $\mathbf{r}_N$) have an equal probability of having been oriented by either end of the tube. This result has profound consequences. For instance, the relative weights of the two competing length scales ξ_1^{Ψ} and ξ_N^{Ψ} will be randomly distributed and not peaked around 1/2, as one might naively expect. This will be the basis for our understanding of the static structure factor of telehelic ionomers.

2.5.3 Radii of Gyration

The radius of gyration is the average distance squared between the different parts of the object and its center of mass. It describes the distribution of matter around the center of mass and therefore gives information on the average size and shape that the end-to-end distance does not provide. It can be measured by various scattering techniques[22-24] in the case of polymers. The parallel ($R_{g\parallel}$) and perpendicular ($R_{g\perp}$) radii of gyration for the three classes of charged chains has been shown to be given by[10]

$$R_{g_\perp}^2 = \frac{Na^2}{12}\langle \sin^2\theta \rangle \tag{32a}$$

$$R_{g_\parallel}^2 = \frac{Na^2}{6}\langle \cos^2\theta \rangle + \frac{N^2a^2}{12}\langle \cos\theta \rangle^2 \qquad for\ Q_1 = -Q_N \tag{32b}$$

$$R_{g\parallel}^2 = \frac{Na^2}{6} \langle\cos^2\theta\rangle + \frac{N^2a^2}{20}\langle\cos\theta\rangle^2 \qquad for\ Q_1 = Q_N \tag{32c}$$

$$R_{g\parallel}^2 = \frac{Na^2}{6} + \frac{Na^2}{12} \langle\cos^2\theta\rangle + \frac{N^2a^2}{30}\langle\cos\theta\rangle^2 \qquad for\ Q_1 = 0;\ Q_N \neq 0 \tag{32d}$$

We will compare our results with these equations below. Note however that eqs 32b and 32c apply only if the charges are of equal magnitude.

2.5.4 Structure Factor for Small Orientation

At low field intensity and/or for $\psi \cong \pi/2$, we have $\xi_i^{\psi} << R_g$ and the chain is almost unperturbed by the field. From eq 27, we then obtain

$$S_{\infty}^{\psi}(q) \approx 1 - \frac{x_1^{\psi}}{6} - \frac{x_N^{\psi}}{6} + \ldots \approx 1 - \frac{x^{\psi}}{3} + \ldots$$

$$for\ (q\,\xi_1^{\psi};\ q\,\xi_N^{\psi}) < qR_g < 1 \tag{33a}$$

$$\approx \frac{1}{x_1^{\psi}} + \frac{1}{x_N^{\psi}} + \ldots \approx \frac{2}{x^{\psi}} + \ldots$$

$$for\ (q\,\xi_1^{\psi};\ q\,\xi_N^{\psi}) < qR_g \wedge qR_g > 1 \tag{33b}$$

where we used $x_1^{\psi} \approx x_N^{\psi} \equiv x^{\psi} \approx x^0 = q^2R_g^2$. We find that the structure factor is almost unchanged

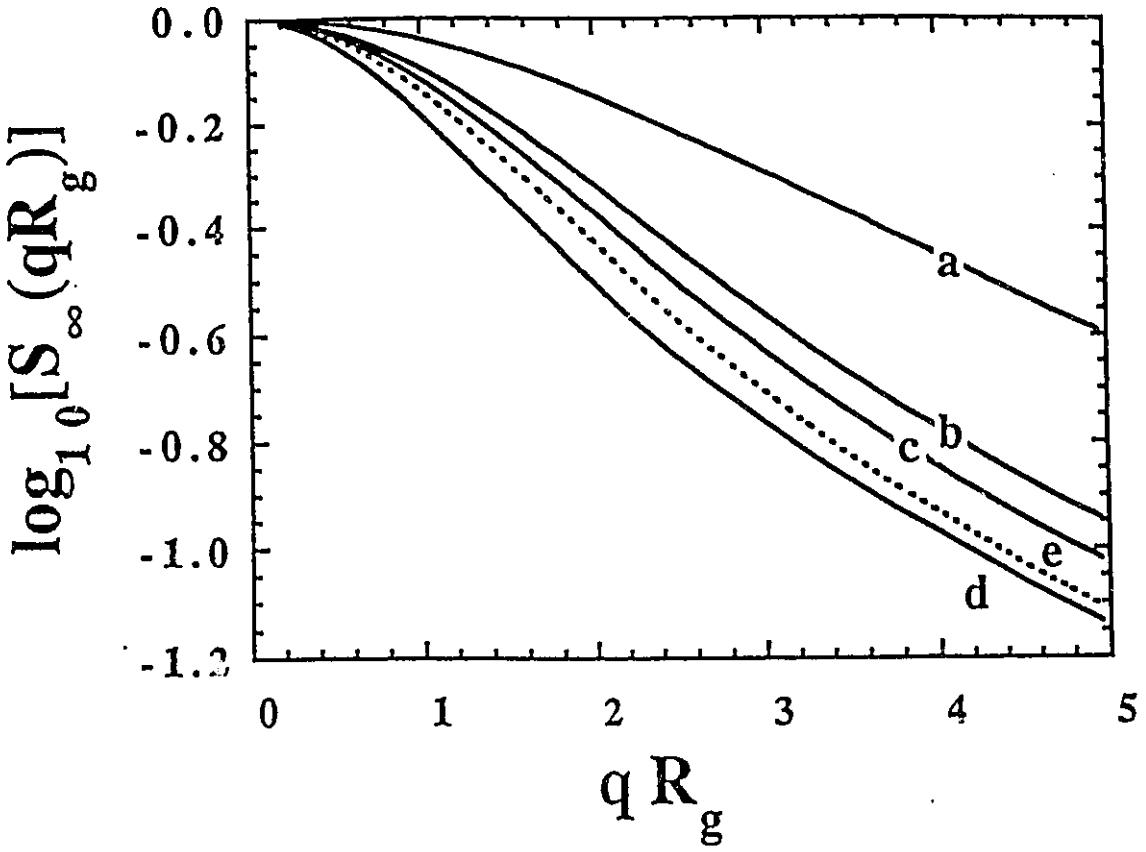

Figure 2. Long-wavelength behavior of the steady-state structure factor $S_\infty^\perp$ (curves a-c), S_{equ} (curve e) and $S_\infty^\parallel$(curve d): log(S) vs. qR_g is plotted for N=1000 and different charged ends. (a) θ_1=10, θ_N=10; (b) θ_1=3, θ_N=-3; (c) θ_1=3, θ_N=0; (d) θ_1=0.05, θ_N=-0.05; (e) θ_1=0, θ_N=0. For small orientations, the chain is almost unperturbed by the field.

compared to eq 21, as shown on Figure 2 for some selected cases. In other words, the radius of gyration is basically unchanged in these limits.

2.5.5 Parallel Structure Factor for High Field Intensities

At fields large enough to have $\xi_i^{\parallel}>>R_g$ for at least one end segment (1 or N), we have to distinguish between four different wavelength regimes.

2.5.5.1 Parallel Structure Factor for $1>q\xi^{\parallel}>>qR_g$

From eq 27, the static structure factor in this regime can then be written as:

$$S_{\infty}^{\parallel}(q) \approx 1 - \frac{(z_1^{\parallel})^2 + (z_N^{\parallel})^2}{30} + \frac{z_1^{\parallel} z_N^{\parallel}}{60} - \frac{x_1^{\parallel}}{6} - \frac{x_N^{\parallel}}{6} + \ldots \tag{34}$$

Since the last two terms are much smaller than the second one, we can neglect them. The third term is zero if only one end is charged. Note that eq 34 reduces to eq 21b when $Q_1=Q_N=0$, as it should be. To simplify, we will now write $Q_1= c\, Q_N$ (with $Q_N>0$ and $|c|\leq 1$), to obtain:

$$S_{\infty}^{\parallel}(q) \approx 1 - \frac{(z_N^{\parallel})^2}{12B^2(c')} + \ldots \approx 1 - \frac{q^2(\xi_N^{\parallel})^2}{12B^2(c')} + \ldots \tag{35a}$$

$$B^2(c') = \frac{5}{2(c')^2 - c' + 2} \tag{35b}$$

$$c' = \frac{\langle\cos\theta\rangle_1}{\langle\cos\theta\rangle_N} \tag{35c}$$

It is easy to show that the structure factor of a rod of length L parallel to **q** is given by

$$S_{\infty}^{I}(q) = \sum_{mn} \exp\{ iq.[R_m - R_n] \} = \frac{2[1-\cos(qL)]}{q^2L^2}$$

$$\approx 1-\frac{q^2L^2}{12} \quad for\ qL<1 \tag{36}$$

Comparing eqs 35 and 36, we can see that the structure factor of our charged chains in the regime $1>q\xi^{I} >>qR_g$ is characteristic of a rod of effective length $\xi_N^{I}/B(c')$ parallel to **q**.

As an example, we now look at three special cases, namely c=-1, c=0 and c=1 ($\xi_1^{I}=\xi_N^{I}=\xi^{I}$ for c=±1; $\xi_1=0$, $\xi_N=\xi^{I}$ for c=0). From eq 35, we get

$$S_{\infty}^{I}(q) \approx 1 - \frac{q^2(\xi^{I})^2}{12} + \ldots \qquad for\ c = -1 \tag{37a}$$

$$S_{\infty}^{I}(q) \approx 1 - \frac{q^2\,((\frac{2}{5})^{\frac{1}{2}}\xi^{I})^2}{12} + \ldots \quad for\ c = 0 \tag{37b}$$

$$S_{\infty}^{I}(q) \approx 1 - \frac{q^2\,((\frac{3}{5})^{\frac{1}{2}}\xi^{I})^2}{12} + \ldots \quad for\ c = 1 \tag{37c}$$

These results agree nicely with the radii of gyration given by eqs 32. Finally, it is interesting to note that eqs 35 predict that the shortest effective rod length $\xi_N^{I}/B(c')$ is found for c'=1/4, and

not for c'=0, i.e., c=0. This means that more compact conformations are predicted when both ends are charged, with $z_1=(1/4)z_N$. This surprising result is due to the competition between the length scales $\xi_N^{\parallel}$ and $\xi_1^{\parallel}$, which, for c'=1/4, tends to form more compact J-like conformations.

2.5.5.2 Parallel Structure Factor for $qR_g<1<q\xi^{\parallel}$

In this regime of intermediate wavelengths, we begin to investigate the chain conformation, but without going to length scales smaller than the equilibrium radius of gyration R_g. Equations 27-29 then indicate that the $S_\infty^{\parallel}(\mathbf{q})$ vs q curves should show some oscillatory behaviour because of the trigonometric functions sin and cos. For the special cases c=±1,0, we get (note that there is only one $x^{\parallel}$ and one $z^{\parallel}$ parameters in these cases)

$$S_\infty^{\parallel}(q) \approx \frac{2\,[\,1-\cos(z^{\parallel})\,]}{(z^{\parallel})^2} + \ldots \qquad for\ c = -1 \tag{38a}$$

$$S_\infty^{\parallel}(q) \approx -\frac{6\sin(z^{\parallel})}{(z^{\parallel})^3} + \frac{6}{(z^{\parallel})^2} + \ldots \quad for\ c = 1 \tag{38b}$$

$$S_\infty^{\parallel}(q) \approx \frac{1}{3} + \frac{2\,e^{-x}\,[\,5x^{\parallel}\cos(z^{\parallel}) - 2z^{\parallel}\sin(z^{\parallel})\,]}{(z^{\parallel})^4} + \ldots$$

$$for\ c = 0 \tag{38c}$$

Figure 3 shows $S_\infty^{\parallel}(\mathbf{q})$ vs qR_g curves for different situations. We first see the steep drop

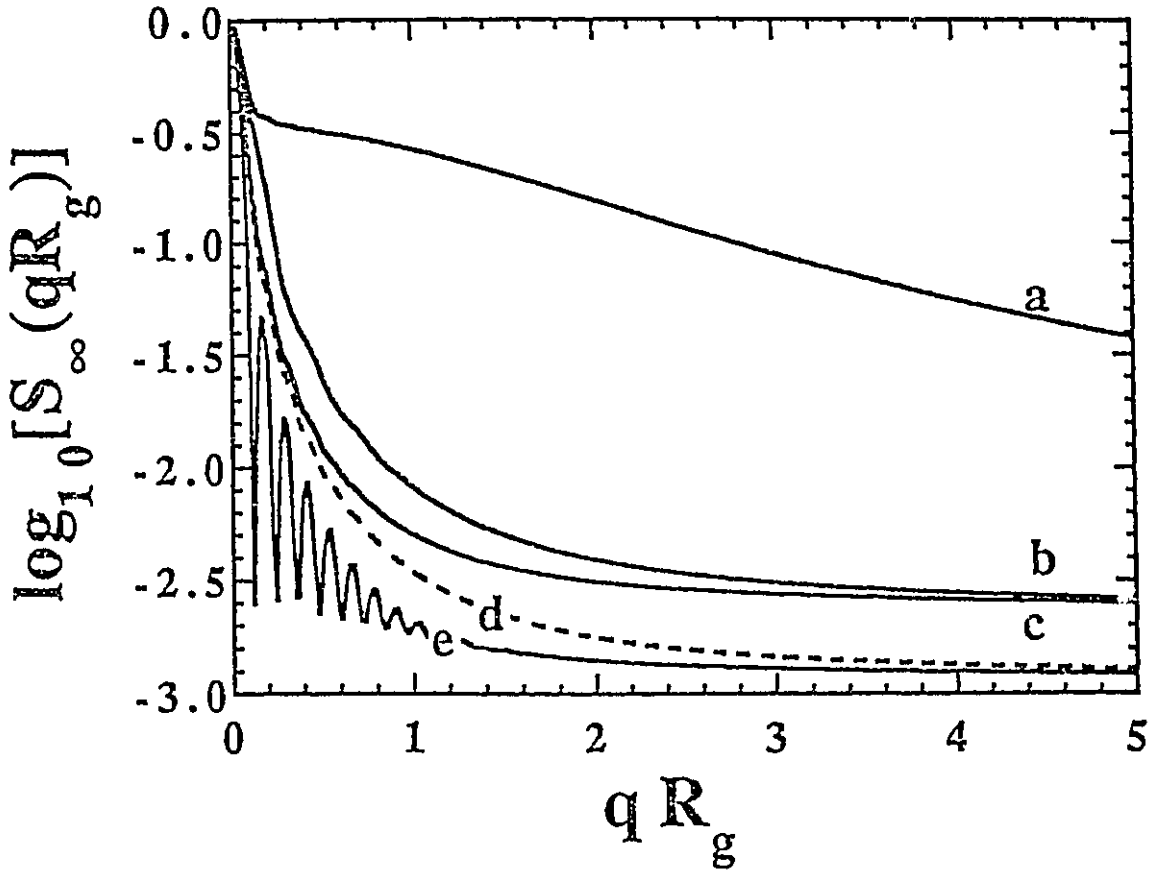

Figure 3. Long-wavelength behavior of the parallel steady-state structure factor: log ($S_{\parallel}$) vs. qR_g is plotted for N=1000 and different end charges. (a) θ_1=0, θ_N=3; (b) θ_1=1, θ_N=3; (c) θ_1=-1, θ_N=3; (d) θ_1=3, θ_N=3; (e) θ_1=3, θ_N=-3. Oscillations appear in the parallel direction only when $\theta_1 \approx -\theta_N$ i.e. for c≈-1.

in the regime $1>q\xi^{\parallel}>>qR_g$ described in section 2.5.5.1. Following this, the structure factor for the three classes of charged chains is very different. For class a chains with $Q_1=-Q_N$ or c=-1, we see clear oscillations in agreement with eq 38a; when $Q_1\neq-Q_N$, however, these oscillations almost disappear. For class b chains, where $1\geq c>0$, the oscillations are always very small; since $z^{\parallel}>>1$, eq 38b does indeed predict negligible oscillations. For class c chains with $Q_1=0$ and $Q_N=Q$, we obtain a very flat line at about $\log[S_\infty^{\parallel}(q)]=-0.52$ (or $S_\infty^{\parallel}(q)=1/3$), in agreement with eq 38c. These results will be explained below using the theorem we introduced in section 2.5.2.

When c<0, the end segments point in opposite directions in an electric field. The average chain then assumes an I-shaped conformation (Figure 1). If $Q_1\neq-Q_N$ however, the electric forces bring in two unequal anisotropic conformation lengths $\xi_1^{\parallel}$ and $\xi_N^{\parallel}$, i.e., the chain is made up of two different parts. Because of the fact that each tube segment has an equal probability of having been oriented by either end segment (section 2.5.2), the distribution function for the curvilinear lengths of each of these two parts is uniform between 0 and L. For a given conformation, the effective length $\xi_\lambda^{\parallel}$ of the chain along the field direction is thus

$$\xi_\lambda^{\parallel} = \frac{\lambda}{L}\,\xi_1^{\parallel} + \frac{L-\lambda}{L}\,\xi_N^{\parallel} \tag{39}$$

where λ is the curvilinear length of the part of the chain oriented by the Q_1 end of the chain. The various molecular conformations simply have different values of λ. The net effective length $\xi_{eff}^{\parallel}$ is thus the average of the lengths $\xi_\lambda^{\parallel}$ over a uniform distribution function for λ:

$$\xi^{l}_{eff} = \langle \xi^{l}_{\lambda} \rangle = \frac{\int_0^L \xi^{l}_{\lambda}\, d\lambda}{\int_0^L d\lambda} = \frac{\xi^{l}_{1} + \xi^{l}_{N}}{2} \qquad (40)$$

Similarly, the structure factor is given by the average of the structure factor for all possible values of λ. For $Q_1=-Q_N$, we have $\xi_{eff}{}^{l}=\xi_1{}^{l}=\xi_N{}^{l}=\xi^{l}$ and there is no competition between two length scales. The structure factor is characteristic of a rod-like chain (compare eqs 38a and 36) and shows a series of oscillations. For $Q_1\neq-Q_N$ however, the structure factor is an average over accessible molecular conformations that have two different orientation lengths $(\xi_1{}^{l},\xi_N{}^{l})$ and two different oscillation periods $2\pi/\xi_1{}^{l}$ and $2\pi/\xi_N{}^{l}$. The result of the superpositon of these oscillations is that no net oscillations exist when $\xi_1{}^{l}$ and $\xi_N{}^{l}$ are very different.

For class b chains, the electric forces attract both ends of the charged molecule to form, on average, a J-shaped conformation (Figure 1). First, we examine the special case where $Q_1=Q_N$. Again, there is only one orientation length $\xi_1{}^{l}=\xi_N{}^{l}=\xi^{l}$. The lengths λ and L-λ of the two arms of the J are uniformly distributed between 0 and L. The structure factor $S_\lambda{}^{l}(\mathbf{q})$ of one J-shaped chain with arm lengths λ and L-λ is easily shown to be given by

$$S^{l}_{\lambda}(q) = \frac{1}{N^2} \sum_{mn} e^{iq\cdot[R_m - R_n]}$$

$$= \frac{2\left[\cos(q\lambda) - 2\cos\left[\frac{q(L-\lambda)}{2}\right] - 2\cos\left[\frac{q(L+\lambda)}{2}\right] + 3\right]}{q^2L^2} \qquad (41)$$

from which the average structure factor is

$$S = \langle S_\lambda \rangle = -\frac{6\sin(qL)}{q^3L^3} + \frac{6}{q^2L^2} \qquad (42)$$

This result is identical to eq 38b with $L \rightarrow \xi^{\parallel}$ and leads to very small oscillations (Figure 3). When $Q_1 \neq Q_N$, we have $\xi_1^{\parallel} \neq \xi_N^{\parallel}$, and a calculation similar to the one leading to eq 42 also shows negligible oscillations. Therefore, the lack of coherence of the resulting scattering functions for each value of λ eliminates all oscillations, even when c=1 (i.e., $Q_1=Q_N$).

For class c, the electric field affects the charged end (i=N) and orients a part of the chain, the rest of the chain staying in a random-walk conformation. As before, section 2.5.2 suggests that the curvilinear length λ of the oriented part is randomly distributed between 0 and L. The effective length of the chain along the field direction is now $\xi_N^{\parallel}/2$. However, since the distance between the segments of the un-stretched, random-walk-like conformation near the uncharged end is much smaller than the distance between all the other segments, the major contribution to the static structure factor comes from this part of the chain. The structure factor for a random-walk chain section with a cuvilinear length λ gives, in the $qR_g<1$ limit,

$$S_\lambda^{\parallel}(q) \approx \frac{1}{N^2}\sum_{mn}^{\lambda/a} e^{iq\cdot(R_m - R_n)} \approx \frac{1}{N^2}\left(\frac{\lambda}{a}\right)^2 \qquad (43)$$

Where we used the fact $\mathbf{q}\cdot(\mathbf{R}_m-\mathbf{R}_n)<<1$. The average over the values of λ gives

$$S^{\perp} = \langle S_{\lambda}^{\perp} \rangle = \frac{1}{3} \tag{44}$$

in agreement with Figure 3 and eq 38c; note that $S_{\infty}^{\perp}=1/3$ for all values of θ_N when $\theta_1=0$.

In conclusion, we find that the theorem described in section 2.5.1 has a profound influence on the scattering behaviour of telehelic ionomers in the wavelength regime where $R_g<1/q<\xi^{\parallel}$. Because the relative weight of the two ends is uniformly distributed between [0,1], the competition between the two end-segments to create new tube sections lead to a polydisperse solution of molecules with a wide range of radii of gyration. The average static structure factor is then featureless, except in the case $c\approx-1$. When only one end is charged (c=0), scattering comes mostly from the unoriented tube sections and we have a remarkably broad plateau at $S_{\infty}^{\perp} \approx 1/3$

.

2.5.5.3 Parallel Structure Factor for $1<q^2R_g^2<q\xi^{\parallel}$

Using the blob sizes $b_i^{\perp}=R_g^2/\xi_i^{\parallel}$ introduced before, this regime can also be defined by

$$\frac{1}{q^2R_g^2}<1<\frac{1}{q\,b_i^{\perp}} \tag{45}$$

The wavelength is thus such that details within a blob cannot be seen ($q^{-1} > b_i^{\perp}$) while details within a distance R_g will be probed ($q^{-1}<R_g$). This means that the blob structure created by a

charged end-segment will show up in the scattering function, while the random-walk nature of the tube segments generated by an uncharged end-segment will also be present. From eq 27, the structure factor in this limit is given by

$$S_{\infty}^{I}(q) \approx \frac{x_1^{I}}{(z_1^{I})^2} + \frac{x_N^{I}}{(z_N^{I})^2} + \ldots \qquad if\ c \neq 0 \tag{46a}$$

and

$$\approx \frac{x_N^{I}}{(z_N^{I})^2} + \frac{1}{x_1^{I}} + \ldots \qquad if\ c = 0 \tag{46b}$$

Using the fact that $x_i^{I}/(z_i^{I})^2 \approx R_g^2/(\xi_i^{I})^2$, we can rewite these equations as

$$S_{\infty}^{I}(q) \approx \frac{6\,(n_1+n_N)}{N} + \ldots \qquad if\ c \neq 0 \tag{47a}$$

and

$$\approx \frac{6\,(n_N)}{N} + \frac{1}{q^2R_g^2} + \ldots \qquad if\ c = 0 \tag{47b}$$

where $n_i = b_i^2/a^2$ is the number of segments contained in a blob of size b_i. Equation 47a thus says that $S_{\infty}^{I}(\mathbf{q})$ should be independent of $\mathbf{q}$ and proportional to the inverse of the number of average blobs forming the chain, $N/(n_1+n_N)$. Figure 3 clearly shows this regime for $qR_g>1$. When only one

end is charged, however, eq 47b indicates that the uncharged end should give rise to a q-dependent term $1/x_1$. This shows as a slowly decreasing function in Figure 3 for $\theta_N=3$ and $\theta_1=0$. Note that the $1/x_1$ term being the largest term in eq 46b, the scattering function for c=0 (one uncharged end) is much larger than with two charged ends ($c\neq 0$). This comes from the fact that a c=0 chain has a very dense end where the random-walk conformation keeps the segments very close to each other, which increases the scattering substantially.

2.5.5.4 Parallel Structure Factor for $1<q\xi^{\parallel}<q^2R_g^2$

In the short wavelength limit where $q^{-1} < R_g^2/\xi^{\parallel} \equiv b^{\parallel}$, with , eq 27 reduces to

$$S_{\infty}^{\parallel}(q) \approx \frac{1}{x_1^{\parallel}} + \frac{1}{x_N^{\parallel}} + \ldots \approx \frac{2}{x^{\parallel}} + \ldots \qquad (48)$$

where $x_1^{\parallel} \approx x_N^{\parallel} \equiv x^{\parallel}$. This result is similar to the one found in section 2.5.4 for low field intensities ($R_g > \xi^{\parallel}$) or for the transverse static structure factor ($\psi=\pi/2$). Therefore, the long-range deformation due to the electric forces acting on the end segments does not affect the molecular conformations on a short length scale such that $q^{-1} < b^{\parallel}$. This is in agreement with section 2.5.

2.5.5.5 Describing the Structure Factor in terms of the Blob Sizes

Now, let us describe the four regimes described in section 2.5.5 in terms of the blob sizes

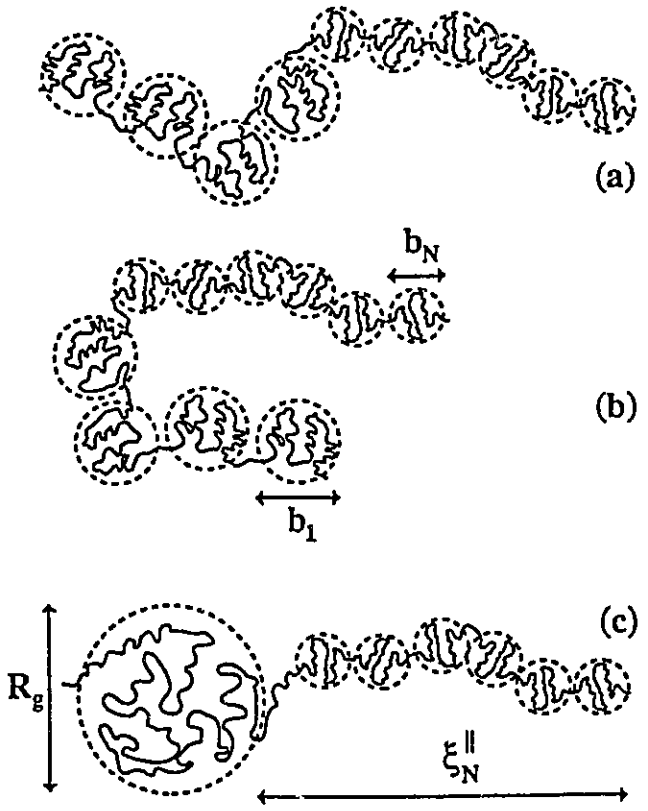

Figure 4. Typical (i.e. average) oriented conformations for the three classes of charged chains with blob sizes b_1 and b_N. (a) $Q_1Q_N<0$: Two kinds of blobs are aligned to form an I shape chain.(b) $Q_1Q_N>0$: Two kinds of blobs are aligned to form an J shape chain. (c) Only one end is charged: One kind of blob (b_N) forms the oriented chain, while the unoriented part has a characteristic size $\approx R_g$.

b_1 and b_N and the anisotropy lengths ξ_1^I and ξ_N^I . Figure 4 represents "typical" (i.e. average) oriented conformations for the three classes of charged chains showing the breakdown of the chain into two sections with blob sizes b_1 and b_N. For $q>(1/b_1;1/b_N)$ (section 2.5.5.4) the electric forces are not strong enough to modify the random-walk nature of the conformation, and the structure factor is that for zero field. In the opposite limit where $q<(1/\xi_1^I,1/\xi_N^I)$ (section 2.5.5.1), the blobs are aligned to form a quasi-rod of average length $\xi^I/B(c')$. For $1>R_g>q>1/\xi^I$ (section 2.5.5.2), the structure factor shows different behaviors for the three types of charged ionomers. When $c<0$ (class a), we obtain strong oscillations only when $Q_1\approx -Q_N$ (or $c\approx -1$). When $c>0$ (class b), we see no oscillation. When $c=0$ (class c), we obtain a flat line around $S_{zz}^I(\mathbf{q})\approx 1/3$. Finally, for $(1/b_1,1/b_N)>q>1/R_g$ (section 2.5.5.3), we probe the blob structure of the rod, which leads to a structure factor that is independent of **q** and proportional to the reciprocal of the number of average blobs; for class c chains, however, the uncharged end dominates and the structure factor still depends on **q** because we then probe inside the random-walk end of the conformation. Of course, the high-field limit characterized by the alignment of the blobs makes sense only if $(b_1,b_N)<R_g$ (i.e. the blobs are smaller than the normal size of the chain) and $(N/n_1,N/n_N)>1$ (i.e. we have a large number of blobs); these conditions are equivalent to $(\xi_1^I, \xi_N^I) >> R_g$ (at least one end segment being charged).

2.5.5.6 The Electric Field Dependence of the Structure Factor

We see from Figure 3 that the $S_{zz}(\mathbf{q})$ vs **q** curves are very much affected by the electric field at $qR_g\approx 1$ because it is in this wavenumber interval that the derivative of the equilibrium

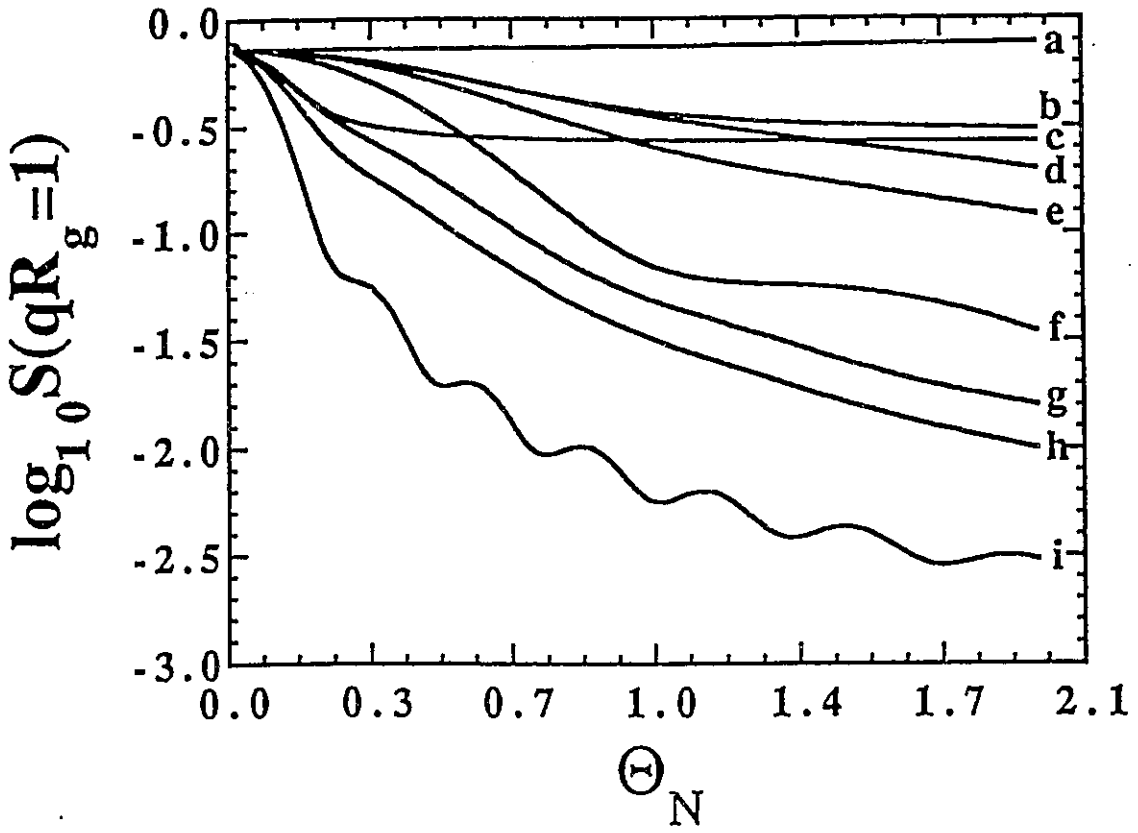

Figure 5. Field dependence of the steady-state structure factor: $\log|S_\infty(qR_g=1)|$ vs. θ_N is plotted for N=1000, different angles ψ and different ratios $c=Q_1/Q_N$ between the end charges. (a) $\psi=\pi/2$, c=-1; (b) $\psi=0$, c=0; (c) $\psi=5\pi/12$, c=0; (d) $\psi=5\pi/12$, c=1/3; (e) $\psi=5\pi/12$, c=-1/3; (f) $\psi=5\pi/12$, c=-1; (g) $\psi=0$, c=1/3; (h) $\psi=0$, c=-1/3; (i) $\psi=0$, c=-1. When $c\neq0$, the chain dimensions are affected at $\psi\neq\pi/2$. When c=0, the structure factor appears as a flat line.

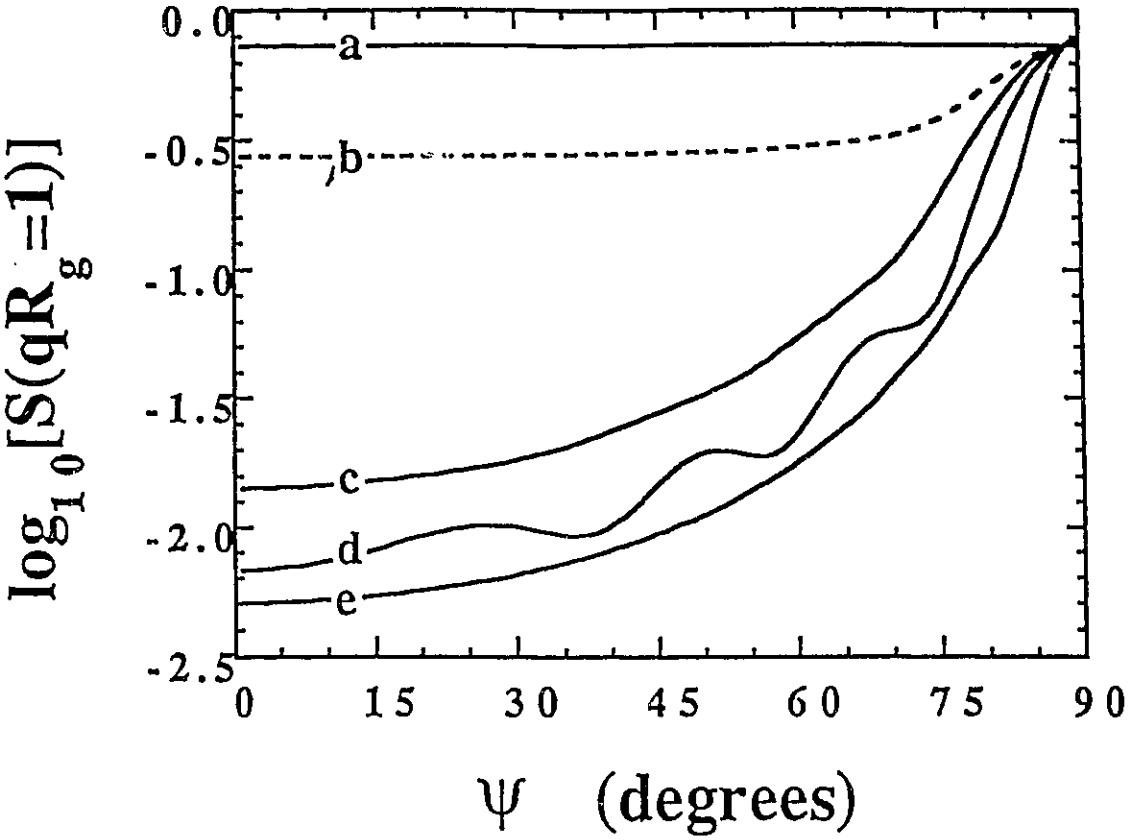

Figure 6. Angular anisotropy of the steady-state static structure factor shown on $\log[S_{ss}(qR_g=1)]$ vs. ψ curves for N=1000 and different end charges. (a) $\theta_1=0$, $\theta_N=0$; (b) $\theta_1=0$, $\theta_N=1$; (c) $\theta_1=1$, $\theta_N=1$; (d) $\theta_1=1$, $\theta_N=-1$; (e) $\theta_1=1$, $\theta_N=-3$. For large angles ψ, the structure factor is the same for all cases since large fields are necessary to modify the structure factor near the transverse direction.

static structure factor $S_{equ}(\mathbf{q})$ is the larger (see curve e on Figure 2).

In Figure 5, we plotted $\log[S_{\infty}(qR_g=1)]$ vs. θ_N for different values of the ratio $c=Q_1/Q_N=\theta_1/\theta_N$ and angle ψ. When $c\neq 0$ (class a and b chains), the effect of the field is dramatic at $\psi\neq\pi/2$ since it leads to oriented conformations of size ξ_{eff}^{ψ}. When $c=0$ (class c), however, most of the scattering comes from those segments near the uncharged end of the molecule. The structure factor is then found to be a flat line (around $\log(1/3)\approx -0.523$) for almost all values of the field θ_N.

In the transverse direction ($\psi=\pi/2$), the average conformation for all classes of charged chains is still random-walk-like, and we need much higher field intensities for the chain dimensions to be affected. Finally, we also notice that some oscillations are present each time the field is such that a peak would appear at $qR_g=1$ on a $S_{\infty}^{\psi}(\mathbf{q})$ vs $\mathbf{qR_g}$ diagram for $c\approx -1$.

2.5.5.7 Anisotropy Induced by the Field

The orientation of the chain in the field direction is accompanied by a slight decrease in its transverse dimensions, and the shape of the average chain conformation is an ellipsoid. Figure 6 shows how the static structure factor measures the properties of this ellipsoid. One can see chain dimensions of the order of R_g only for large angle ψ. We also see some oscillations when $c\approx -1$ and a remarkably flat line (around $\log_{10}(1/3) = -0{,}523$) for $c=0$. Of course, individual conformations (which can be observed by various video-microscopy techniques[7,18]) are expected to be anisotropic even in absence of electric forces, i.e. even if the average conformation is isotropic[19]; the orientation and anisotropy effects discussed here refer to average molecular conformation properties such as those observed by scattering.

Chapter 3

Discussion

In the biased reptation model[4-5], originally developed to study DNA gel electrophoresis, the reptating molecule experiences two biases in the presence of an electric field. Firstly, the molecule tends to orient in the field direction because of the electric forces acting on the end segments of the primitive chain. Secondly, the total force on the molecule leads to a net electrophoretic velocity. These two biases are "coupled" because the charge is uniformly distributed along the DNA chain; also, the tube orientation increases the electrophoretic velocity[4,5,13]. The charges on the end segments have a major impact during reptation since they alone generate the new tubes in which the migration occurs. For example, it was recently shown that reducing the charge on the ends of DNA molecules could greatly increase the separation power of gel electrophoresis[13]. In this article, we studied the opposite situation where the polymer has charges only on or near its ends, hence the name telehelic ionomers.

The electrophoretic migration of these telehelic ionomers in neutral gels, or in dense solutions of neutral polymers, should be very well described by the biased reptation model used here. For example, the absence of charges along the main backbone of the molecule eliminates the growth of hernias and other no-reptation molecular conformations that violate the tube description[20]. Also, the negligible electrophoretic velocity (see next paragraph) will eliminate the "bunching" effect found during DNA gel electrophoresis[20].

In our calculation, we assumed that prob $[\eta(t)=+1]$ = prob $[\eta(t)=-1] = 1/2$ in the Langevin equation of motion (1). When this is not the case, an extra term[11] appears in eq (11) and subtle

effects may occur, such as those leading to band inversion during DNA gel electrophoresis[21]. This term, and the corresponding field-driven electrophoretic velocity, can be neglected for long telehelic ionomers when tube renewal is due mostly to the unbiased longitudinal Brownian motion of the chain along its tube axis. For a tube of length Na, the Brownian tube renewal time is simply given by[16,17]

$$\tau_D = N^2 \Delta t \tag{49}$$

where Δt is the average time required by the chain to move over a distance a. The average electric force acting along the tube axis due to a charge Q on one end segment is given approximately by

$$\langle F_1 \rangle \approx QE \langle \cos\theta \rangle \tag{50}$$

which leads to the field-driven tube renewal time

$$\tau_E \cong \frac{Na}{\langle F_1 \rangle / \xi_1} \tag{51}$$

where $\xi_1 = 2k_B T \Delta t / a^2$ is the curvilinear friction coefficient of the chain in its tube. The longitudinal velocity and bias can thus be neglected if

$$\frac{\tau_E}{\tau_D} \approx \frac{3}{N\theta^2} \gg 1 \tag{52}$$

For experimental values such as Q=10e, E=10V/cm, a=10nm, T=300K, we obtain a scaled field $\theta^2 \approx (QEa/2k_BT)^2 \approx 4x10^{-6}$ and eq 52 requires that $N<8x10^5$ segments. These values are typical of DNA electrophoresis in polyacrylamide gels. Therefore, we can easily neglect the electrophoretic velocity of telehelic ionomers in most experimentally relevant situations since the Brownian motion dominates the small field-driven longitudinal drift.

When the electrophoretic velocity is negligible, the molecule migrates through normal Brownian motion, and the shape of the molecule is a function of the properties of the tube-creating end-segments. This is why the static structure factor $S_{\alpha}(q)$ is found to be a function of the boundary condition parameters $x_{1,N}$ and $z_{1,N}$. The boundary conditions lead to a competition between different length scales. On the one hand, the tendency to optimize the entropy of the molecular conformations is related to the radius of gyration R_g and to the parameters $x_{1,N}$. On the other hand, charged end-segments tend to orient the molecular conformations in the direction of the applied electric field, which leads to the orientation lengths $\xi_{1,N}$ and the parameters $z_{1,N}$. When $\xi^{1}>R_g$, the electric forces substantially deform the molecular conformation. The physics of this effect can be understood quantitatively using two fundamental concepts: (i) charged ends create random-walk blobs of tube sections that align themselves in the field direction; (ii) the number of tube sections created by a given end segment is uniformly distributed between 0 and N, the total length of the molecule. The latter fact has a profound impact of the scattering structure factor of reptating telehelic ionomers. For instance, except for the case where $Q_1=-Q_N$, we virtually obtain a polydisperse solution of molecules; each molecule is formed of two types of blobs, but the number of such blobs varies randomly from one molecular conformation to another.

Perhaps the most remarkable example of this polydisperse-like behaviour is found for molecules with charges only at one end. In this case, our results predict that we should see a rod-like structure for long wavelengths but a random-walk structure at intermediate wavelengths $q^{-1}>\xi^{I}$. This leads to a step-like $S_{\infty}^{I}(\mathbf{q})$ vs $\mathbf{q}$ curve that is totally different from any curve obtained for molecules having charges on both ends.

In fact, our results suggest a straightforward way to measure the ratio $c=Q_1/Q_N$ between the charges on the two ends of telehelic ionomers. Firstly, for fields small enough that $\Theta_{1,N}<1$, eqs 34, 13b and 6b lead to

$$A \equiv \lim_{q\to 0} \frac{1-S_{\infty}^{I}}{q^2} = \frac{L^2E^2a^2}{2160\,(k_BT)^2}\,(2Q_1^2+2Q_N^2-Q_1Q_N) \tag{53}$$

where A is independent of q. Secondly, from eq 46a we obtain, in the specified regime,

$$B \equiv S_{\infty}^{I}(q) = \frac{6\,(k_BT)^2}{E^2La}\,(\frac{1}{Q_1^2}+\frac{1}{Q_N^2}) \tag{54}$$

which is also independent of q. Finally, from eqs 21b and 33a we get

$$F \equiv R_g^2 = \lim_{\substack{E\to 0\\ q\to 0}} \frac{3\,(\,1\,-\,S(q)\,)}{q^2} \tag{55}$$

From eqs 53 -55, we find that the ratio $c = Q_1/Q_N$ is the solution of

$$2c^4 - c^3 + (4 - 60\frac{AB}{F})\, c^2 - c + 2 = 0 \qquad (56)$$

This equation is valid only if $\xi_1^I > R_g$ and $\xi_N^I > R_g$. Since A, B and F can all be measured experimentally, eq 56 can be used to obtain the ratio $c = Q_1/Q_N$. This could be a way to better characterize a sample of telehelic ionomers.

Adding a few electric charges to the ends of long neutral polymers provides a simple way to orient them in a matrix. Although their electrophoretic velocity is negligible, the reptation mechanism allows the user to orient them using an external electric field. The orientation time is given by eq 49. Note however that unless $Q_1 = -Q_N$, one cannot have a uniform molecular orientation.

In conclusion, we have studied the orientation properties of reptating telehelic ionomers. Such molecules can be synthesized (see ref.(10) for some details concerning the chemistry involved). The key to understanding the results of our analytical calculations of the static structure factor is provided by the theorem presented in section 6.2. Unless $Q_1 = -Q_N$, these molecules can be in a wide range of oriented conformations that leads to an average behaviour characteristic of a polydisperse solution. When only one end is charged, the static structure factor has a unique step-like shape. Finally, we showed that scattering expirements can be used to measure the charge ratio $c = Q_1/Q_N$. These experiments would be a good test for the reptation model.

Part II

Reptation, Entropic Trapping, Percolation and Rouse Dynamics of Polymer Chains in "Random" Environments

Chapter 1

Introduction

Macromolecules play a central role in chemical technology and indeed in biology. The study of the dynamics of polymers in the liquid state (the dynamics of polymer solutions and melts) has been expanding at a very rapid pace in the last few decades. It has become possible to offer theories which explain the salient features of macromolecular solution systems.

The motion of a polymer in dilute solutions is fairly well understood in terms of the simple Rouse model. In this formalism, the interaction between separate polymer chains is neglected, and the interaction between the polymer chain and the solvent is treated in terms of a friction coefficient and (in the Zimm version of the theory) a hydrodynamic theory[25]. For the Rouse model, the diffusion coefficient of the center of mass of the chain D and the chain relaxation time τ depend on the chain length M according to $D \sim M^{-1}$ and $\tau \sim M^{2}$. On the other hand, the dynamics of long flexible polymers in concentrated solutions and melts can be described by the reptation model. Since the entanglements become dominant and force the polymer to reptate, the scaling laws become $D \sim M^{-2}$ and $\tau \sim M^{3}$. Furthermore, the dynamics of polymers through porous media such as in gel permeation chromatography, enhanced oil recovery membrane separations, and ultrafiltration, is again altered because entanglements with different chains are negligible while the environment itself is non-uniform.

In general, porous media have very complicated random interconnected pore structures. The fundamental issue in these problems is the transport of a polymer chain from a region of large volume where the chain entropy is higher to another region of small volume where the

chain entropy is lower. Thus the polymer chain moves across an entropic barrier. In order to understand this complex problem, Muthukumar and Baumgartner[26-28] introduced a simple but well-defined model of polymer diffusion in porous systems.

Muthukumar and Baumgartner reported that polymer chains can be entropically trapped in "random" environments. Under these conditions, their diffusion coefficient was found to decrease very quickly with molecular size, in agreement with the model which predicts that diffusion is then governed by narrow passages which reduce the entropy of the molecules when they try to move between the large "pores" of the random system. These authors observe evidence of this new phenomenon in computer simulations of the dynamics of non-self avoiding[26] as well as self-avoiding[27] chains in "random" environments composed of monomer-size obstacles (placed randomly in space at a concentraton below the percolation limit) or large empty boxes connected by narrow channels[28]. Hoagland et al[29,30]. and Mayer et al[31]. observed a new regime of gel electrophoresis where the mobility of long polyelectrolytes decreases quickly with molecular size; both groups interpreted these results, which cannot be explained by any other model of gel electrophoresis, as an indication that polyelectrolytes like DNA can get entropically trapped in the large pores of the "random" gel (polyacrylamide).

However, the concept of a "random" environment is ill-defined and the conditions under which entropic trapping may actually occur are not clear. Moreover, the transition from entropic trapping to Rouse or Reptation dynamics is still not understood. The simulation conditions used by Muthukumar and Baumgartner cannot be used to infer the dynamics of polymer chains in real gels as their "random" environments lack realism. For instance, their percolation lattice of block-obstacles does not support its own weight.

In the second part of this thesis, we study the dynamics of polymer chains in imperfect periodic arrays of obstacles. Our original goal was to find the minimum degree of randomness one needs to observe entropic trapping of long polymer chains. We find that entropic trapping starts as soon as pores that are big enough to "trap" entire molecules form, as expected. However, our results differ substantially from those of Muthukumar and Baumgartner because the large pores are then very far from one another; as a result, the diffusion coefficient is found to actually decrease when the concentration of obstacles is reduced, a counter-intuitive result of entropic trapping that had never been reported before. Also, we find that entropic trapping disappears when the obstacles cease to form a percolating cluster that can obstruct polymer motion. Finally, we show the first clear pictures of entropic trapping using density plots to give the reader an intuitive understanding of the process and the formation of percolation pathways through the system.

Chapter 2

Algorithm and Simulation Results

In order to obtain a good understanding of the dynamics of entropically trapped polymer molecules, we decided to study the problem in two-dimensions. As we will show below, this will allow us to map the motion of the molecules using contour or density plots and to estimate the degree of localization of the polymers. We thus use the bond-fluctuation algorithm recently proposed by Carmesin and Kremer[32] since it is the only one that gives the right Rouse dynamics for a two-dimensional self-avoiding polymer in a dense system.

2.1 The Bond-Fluctuation Algorithm

This algorithm keeps the advantages of the simple lattice models and overcomes the drawbacks of the most popular Verdier-Stockmayer model[32]. In this algorithm, polymers of length M consist of M monomers connected by M-1 bonds. The number of monomers (bonds) is fixed. The polymers move on a square lattice with lattice constant 1 (in computer units), and each monomer occupies the four lattice sites of a unit cell. To avoid bond cuts, the bond length has to be smaller than 4 (see Figure 7). At each step in the evolution of the system a randomly chosen square-monomer moves to a randomly chosen nearest neighbour lattice cell. The acceptance of a move is subject to satisfy both the bond length restriction and the self-avoiding walk (SAW) or excluded volume condition. Since two monomers can never touch and each bond is shorter than 4 unit long, two bonds can never intersect and self-avoidance is enforced.

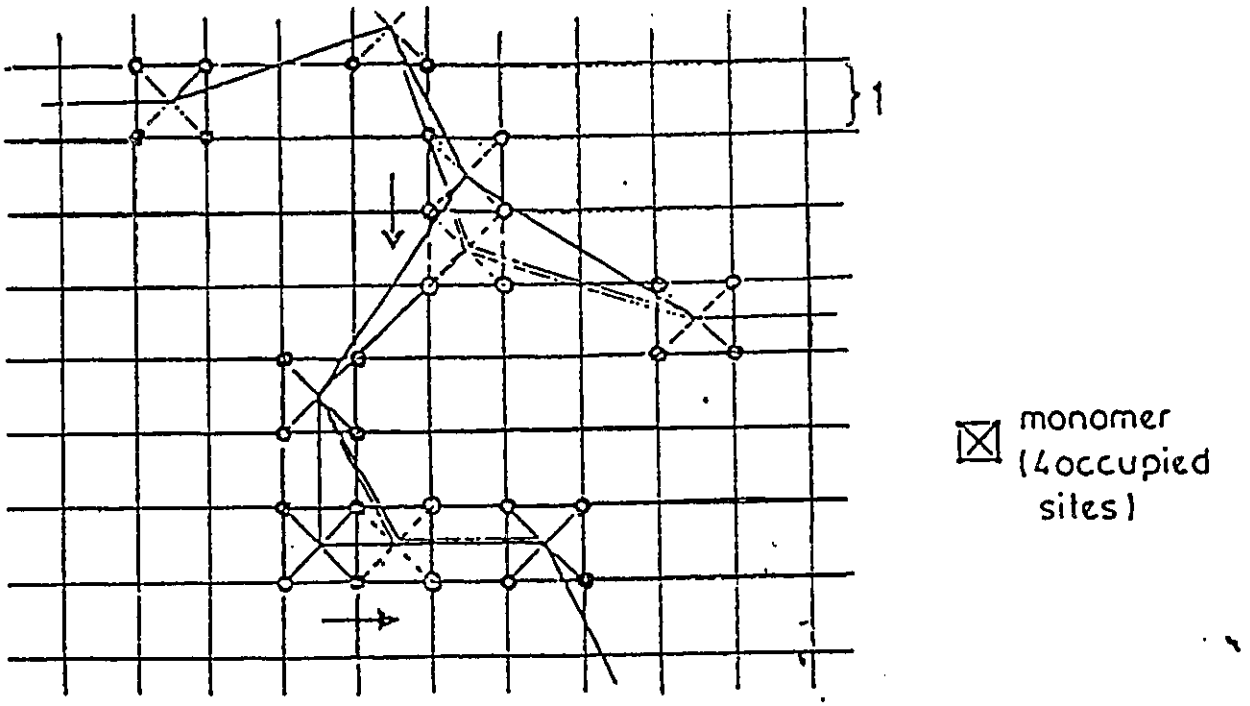

Figure 7. Illustration of the bond fluctuation method. Two typical moves are indicated. Monomers cannot touch and bond length must be small or equal square root 3 in order to have correvt exclude volume effects.

In our simulation, the obstacles are represented by single cells like the monomers themselves. The obstacles form a periodic lattice of lattice parameter q. Note that q must be larger than 3 in order to use the bond-fluctuation algorithm. The results presented here were obtained for q=4. A fraction c of the obstacles is removed randomly from the 840×840 lattice and periodic boundary conditions are used. The initial polymer conformation is prepared by a long warm-up period, as usual. For c=1, the q=4 lattice of obstacles corresponds to a chain moving in a tight tube and reptation behaviour[33] is found for molecules as small as M=5 (each reptation segment corresponds to about 2-3 monomers for q=4). The simulation were carried out on IBM RS/6000 and SUN workstations using Fortran codes. Figure 8 shows a number of typical polymer conformations found during a simulation.

The main properties we are interested in are the center-of-mass diffusion coefficient D, the autocorrelation (or terminal relaxation) time τ of the end-to-end vector **h** of the chain, and the mean-square radius of gyration R_g^2. The three properties are defined as follows:

(1) the center-of-mass diffusion coefficient D

$$D = \lim_{t\to\infty} <[R_{cm}(t)-R_{cm}(0)]^2>/4t \qquad (1)$$

where the $\mathbf{R}_{cm}(t)$ and $\mathbf{R}_{cm}(0)$ denote the position vectors of the center-of-mass at time t and 0, respectively. Usually, we define the mean square displacement $R^2(t)$ as

$$R^2(t) = \langle\, [R_{cm}(t) - R_{cm}(0)]^2 \,\rangle \qquad (2)$$

Equation(1) can then be rewritten as

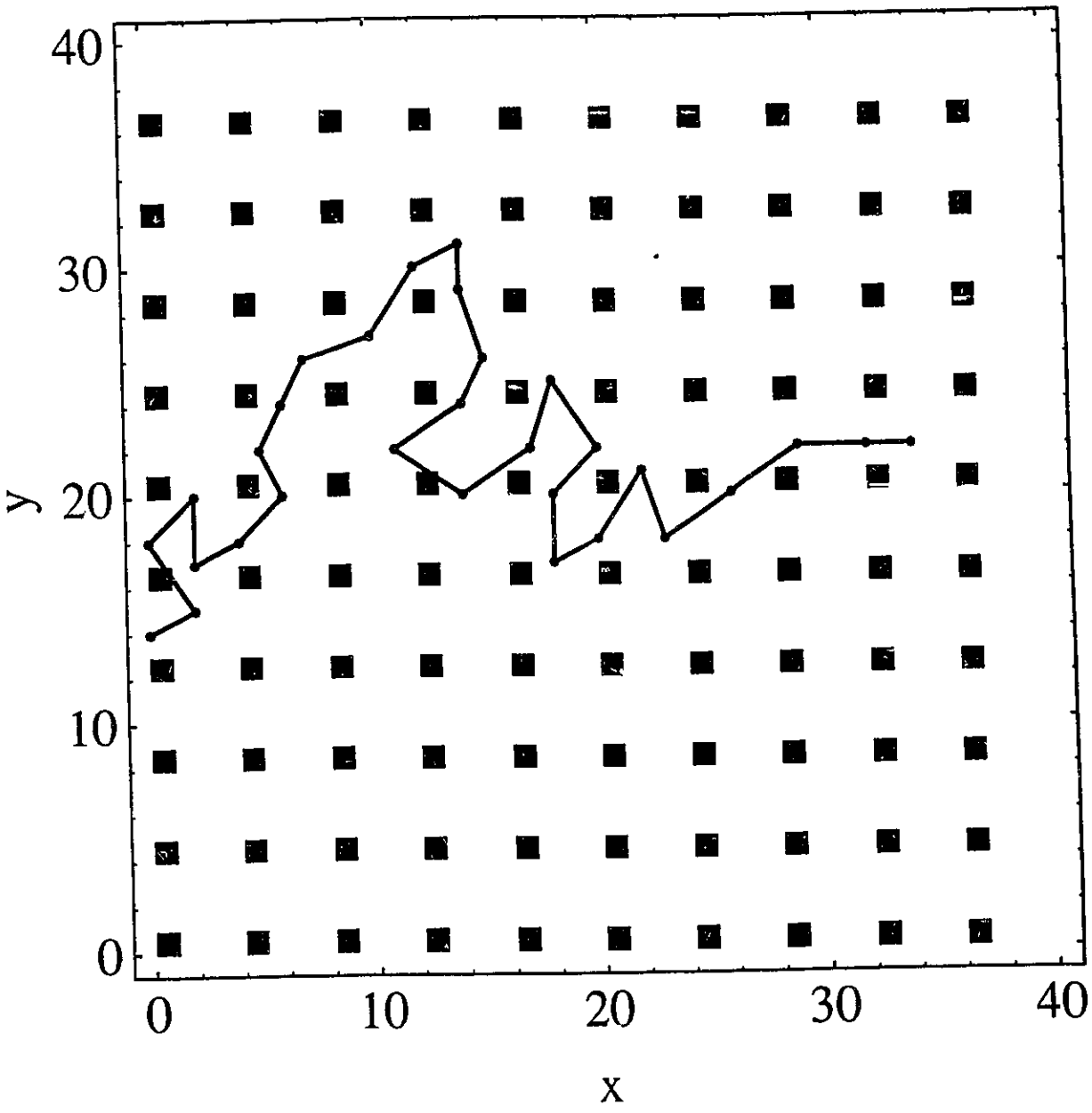

Figure 8. Typical polymer (length M=30) conformations of a number of systems during simulation. The small dark squares represent the obstacles. (a) c=1: The obstacles form 2-D regular array. The chain reptates through the obstacles.

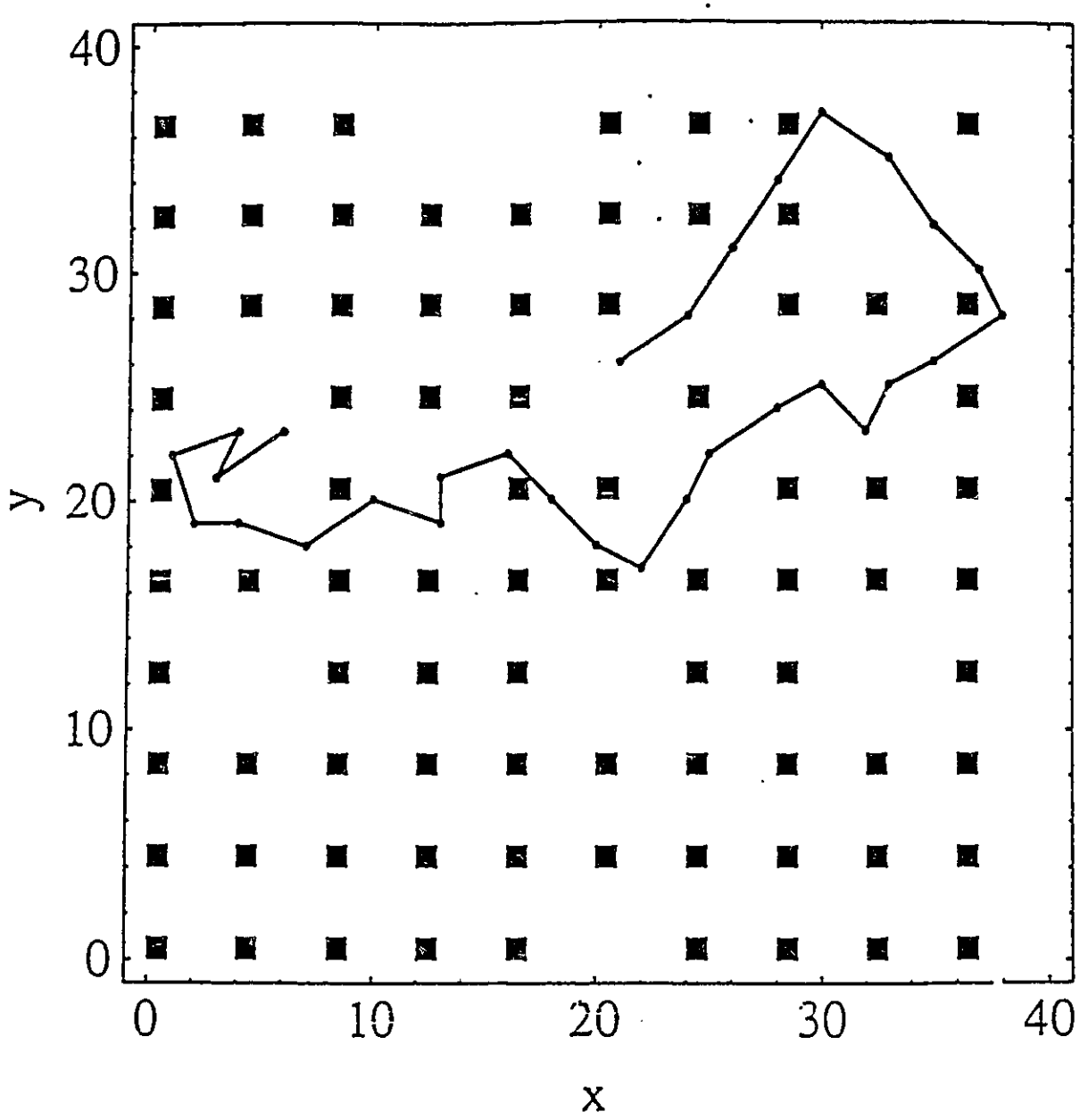

(b) c=0.8.

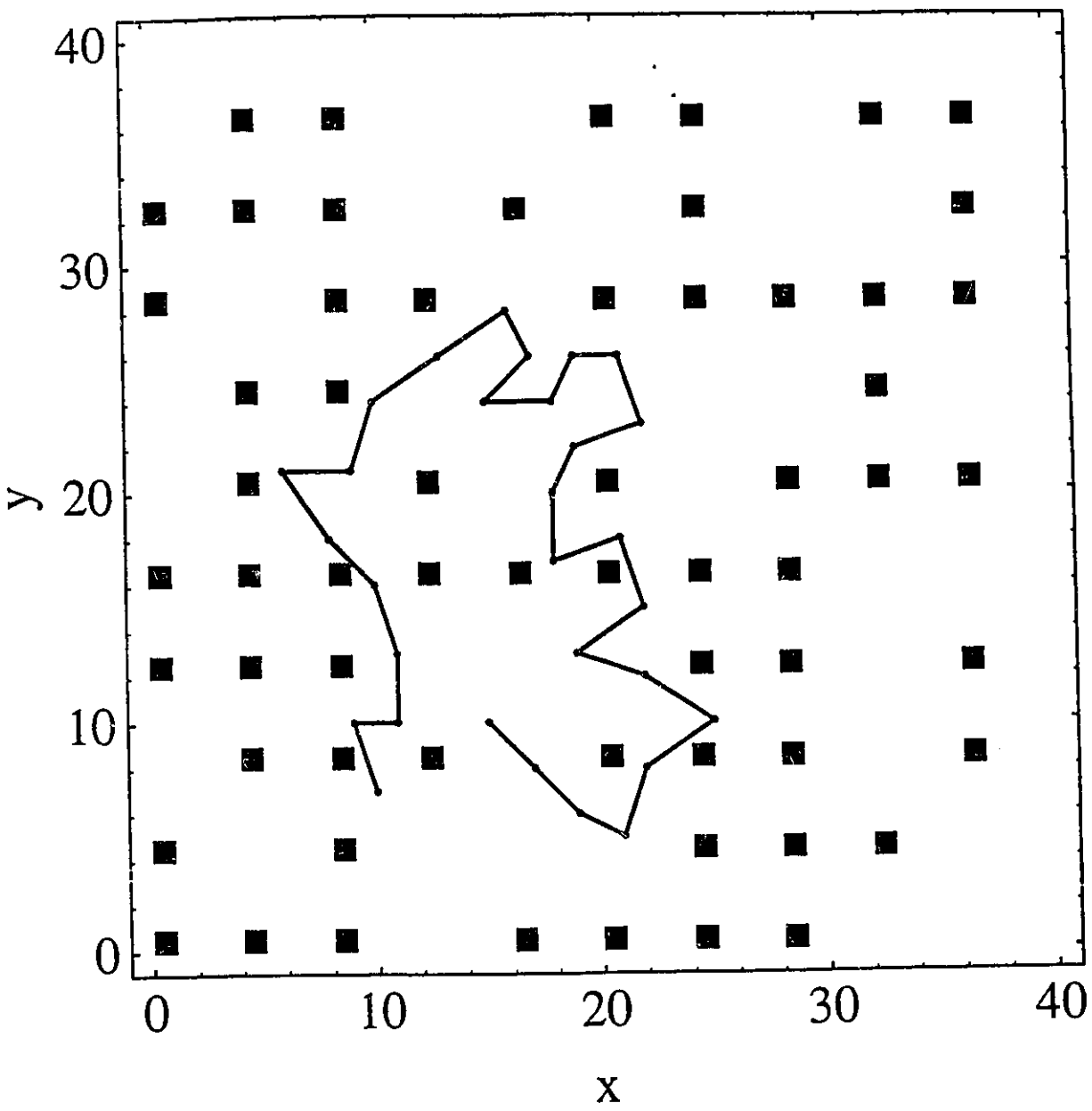

(c) c=0.6.

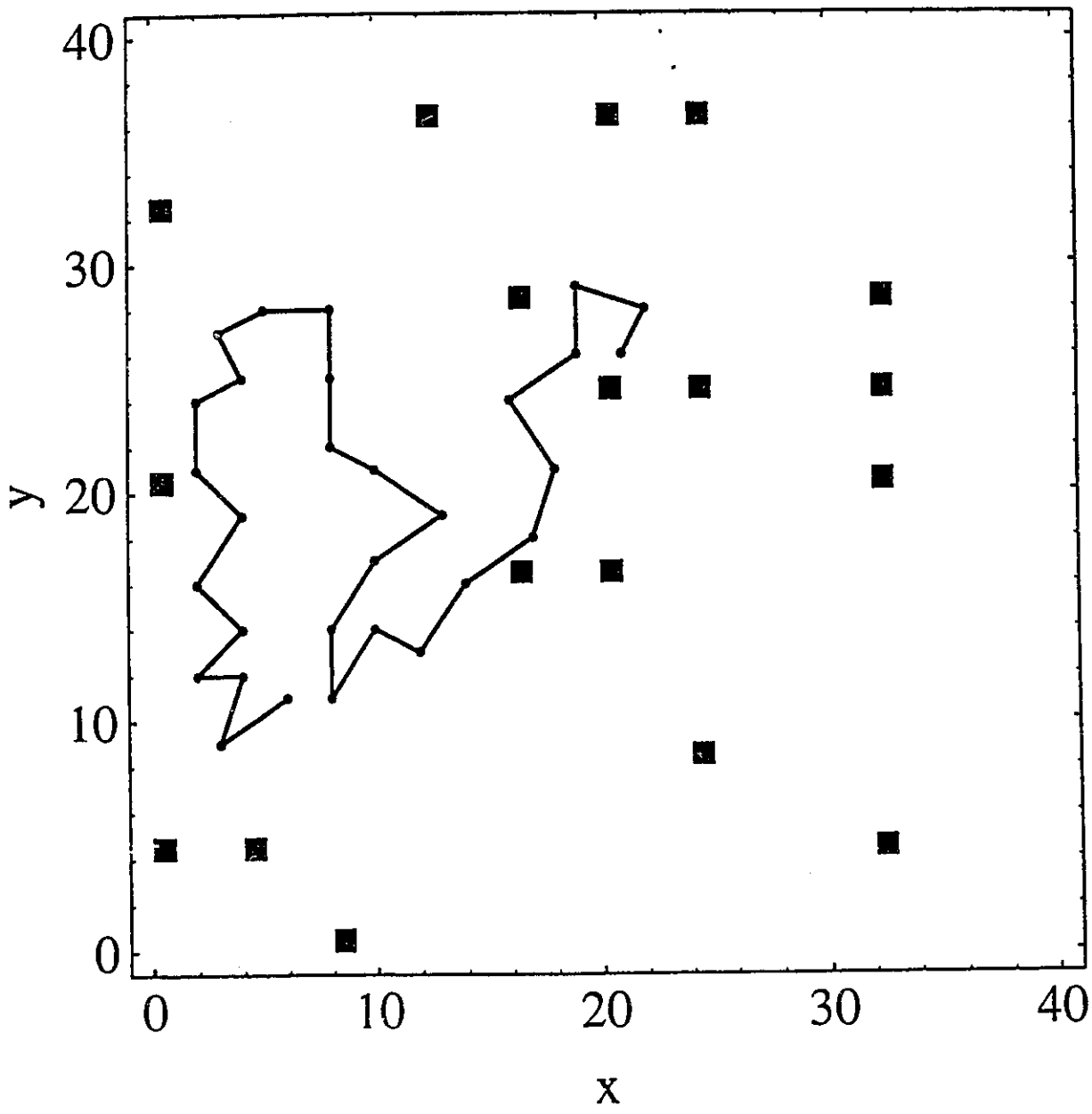

(d) c=0.2.

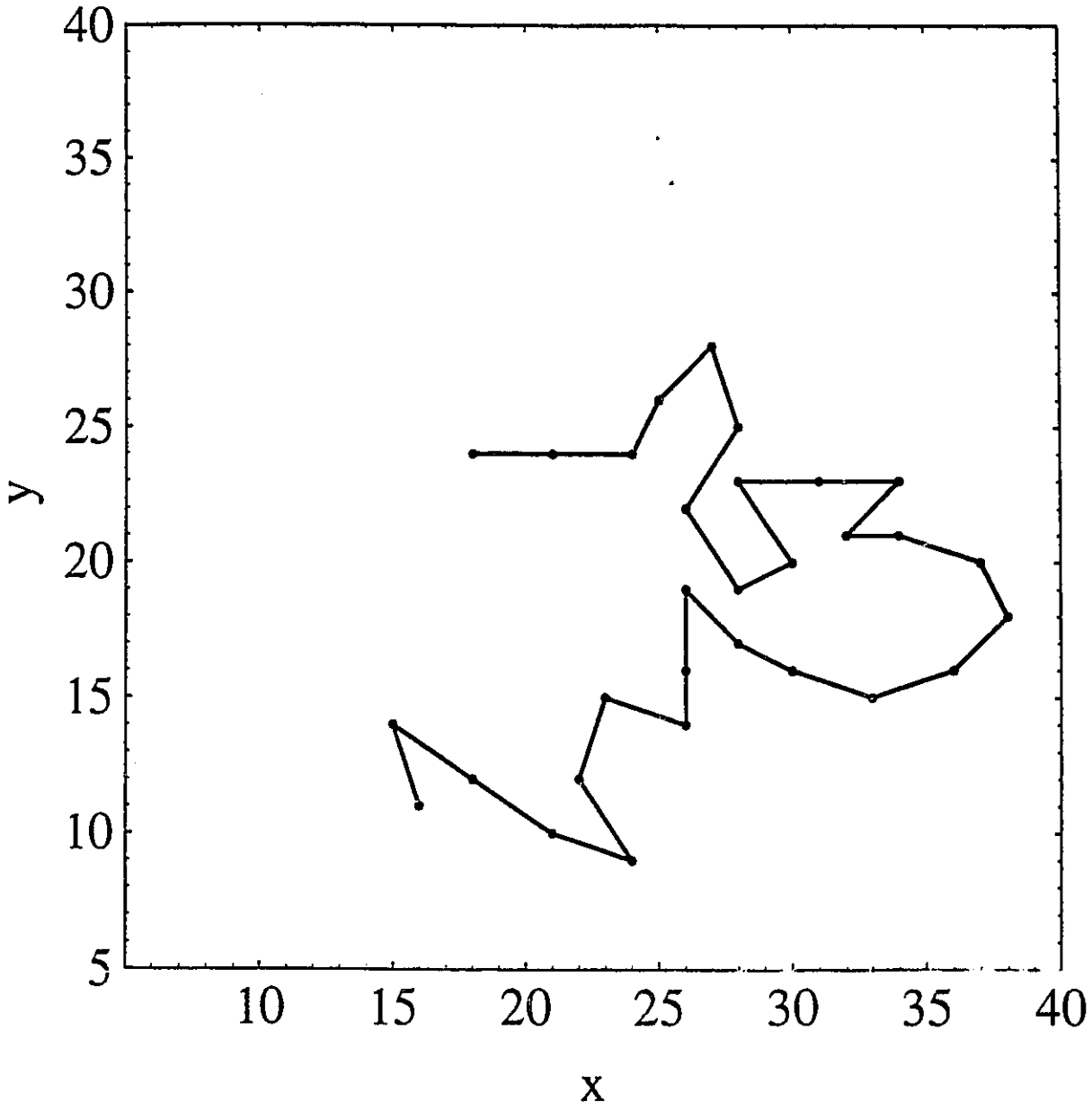

(e) c=0: There is free and we recover the Rouse limit.

$$D = \lim_{t\to\infty} \frac{1}{4}\frac{d}{dt}R^2(t) \tag{3}$$

This shows that D is proportional to the slope of the curve of the mean-square displacement vs. time, taken at long times. Also, D can be obtained as the intercepts of the log-log plot of $R^2(t)$ vs t.

(2) the longest or terminal relaxation time τ

$$\frac{\langle \boldsymbol{h}(t)\cdot\boldsymbol{h}(0)\rangle}{\langle h^2(0)\rangle} \sim \exp(-t/\tau) \tag{4}$$

where **h(t)** and **h(0)** are the end-to-end vectors at times t and 0 and τ is the terminal relaxation time of this autocorrelation function. This relation is valid for long times since multiple short time scale relaxation processes also take place for shorter times.

(3) the mean square radius of gyration R_g^2

$$R_g^2(M) = \frac{1}{M}\left\langle \sum_{i=1}^{M} (\boldsymbol{R}_i - \boldsymbol{R}_{cm})^2 \right\rangle \tag{5}$$

with

$$\boldsymbol{R}_{cm} = \frac{1}{M}\sum_{i=1}^{M} \boldsymbol{R}_i \tag{6}$$

where R_i is the position vector of i-th monomer.

2.2 The Rouse and Reptation Limits

When the concentration is zero in our system, it corresponds to a free chain moving on the two dimensional lattice. The dynamics of the chain should then obey Rouse dynamics. According to the scaling laws given by Carmesin and Kremer[32], one should have $D \sim M^{-1}$ and $\tau \sim M^{2.5}$ for a SAW chain, and $D \sim M^{-1}$ and $\tau \sim M^{2}$ for a RW (random walk) chain. Carmesin and Kremer tested the static and dynamic properties of both SAW and RW chains with the bond fluctuation algorithm. The above mentionned power laws were clearly established. Also, our simulation results for free SAW chains are in good agreement with theirs. On the other hand, when the concentration is c=1, the system corresponds to a chain moving through a periodic array of obstacles, and one expects reptation dynamics with $D \sim M^{-2}$ and $\tau \sim M^{3}$ for both SAW and RW chains. We did this situation test as well and the result is $D \sim M^{-1.9}$ and $\tau \sim M^{3.1}$. These results are in excellent agreement with the theoretical predictions; the slight differences are due to finite size effects that exist for small chains. The reason why SAW and RW chains show the same reptation behaviour is that the excluded-volume effect is screened out in a dense system.

2.3 The Simulations

We have studied the static property R_g^2 and the dynamic properties D and τ for polymer chains moving in random environments. The three properties were computed after very long simulation runs. For the dynamic properties D and τ, we save the position vectors of the center-of-mass, $\mathbf{R}_{cm}(t)$, as well as the end-to-end distance vector, $\mathbf{h}(t)$, by writing to a file at regular

intervals Δt (time is measured in number of Monte Carlo steps per monomer, as usual) during the simulation of a single chain. This file has a amount data (typically 10^4 to 10^5 lines). The static physical quantity R_g^2 is obtained by averaging over the whole run.

Now, we give the methodology to analyze this huge data file. Consider the mean square displacement $\mathbf{R^2(t = j\ \Delta t)}$ and assume we have the position vectors of the center-of-mass stored in a file for discrete times k Δt. We can approximate the ensemble average eq 2 for the mean square displacement as

$$R^2(j\ \Delta t) = \frac{1}{M}\sum_{k=1}^{N(j)}\left(R_{cm}([jk+1]\Delta t) - R_{cm}([jk-j+1]\Delta t)\right)^2 \tag{7}$$

where N=N(j) is the total number of groups of j lines we can get from the data file, i.e. the size of the ensemble for this specific time scale t:

$$M=Integer[\frac{s-1}{j}] \tag{8}$$

where s is the number of lines in the data file. Since the ensemble size N decreases with increasing j, the statistics gets poorer when time (i.e. j) increases. Figures 10 and 11 clearly show this effect. To illustrate this method, Fig. 9 provides the flow chart to calculate the mean square position for j=3 or t=3 Δt. We use a similar method to analyze the end-to-end vector data file.

We should mention here that the CPU time taken for obtaining the simulation data file for **R(t)** is much longer than that for obtaining **h(t)**. We give much shorter regular intervals for running the end-to-end distance file since the relaxation time τ is defined as the time required for the onset of the long time diffusion.

As an example, Figure 10 shows a log-log plot of the mean square displacement $\mathbf{R^2(t)}$

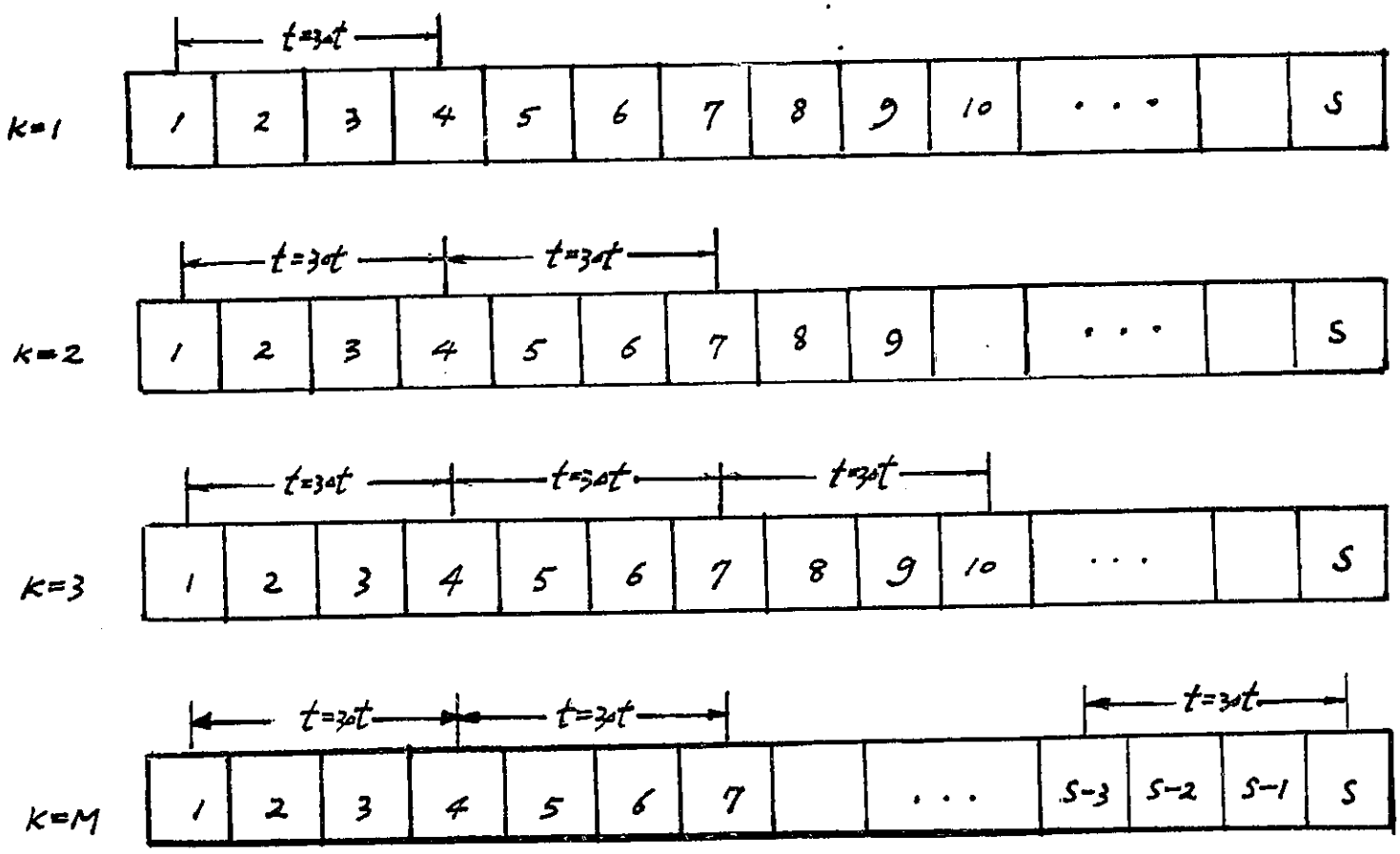

Figure 9. Flow chart of a data file with s lines, showing cuts in sampling as the calculation of a time correlation function. Here the calculation is for the t=3 Δt, and the ensemble size N is related to s and j by eq 8.

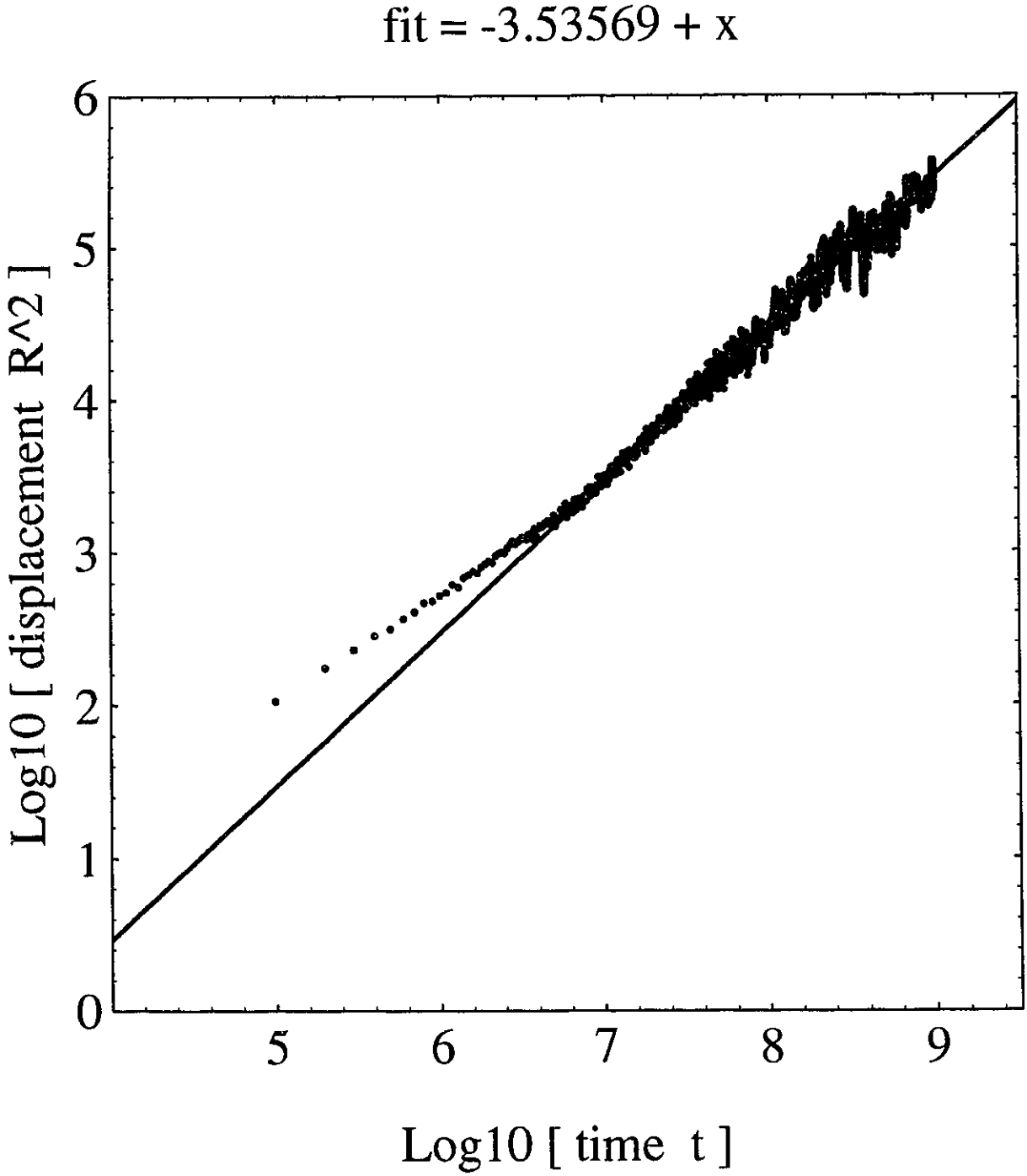

Figure 10. Typical log-log plot of the mean square displacements $R^2(t)$ of the center of mass vs time t for a chain M=20 and c=0.8.

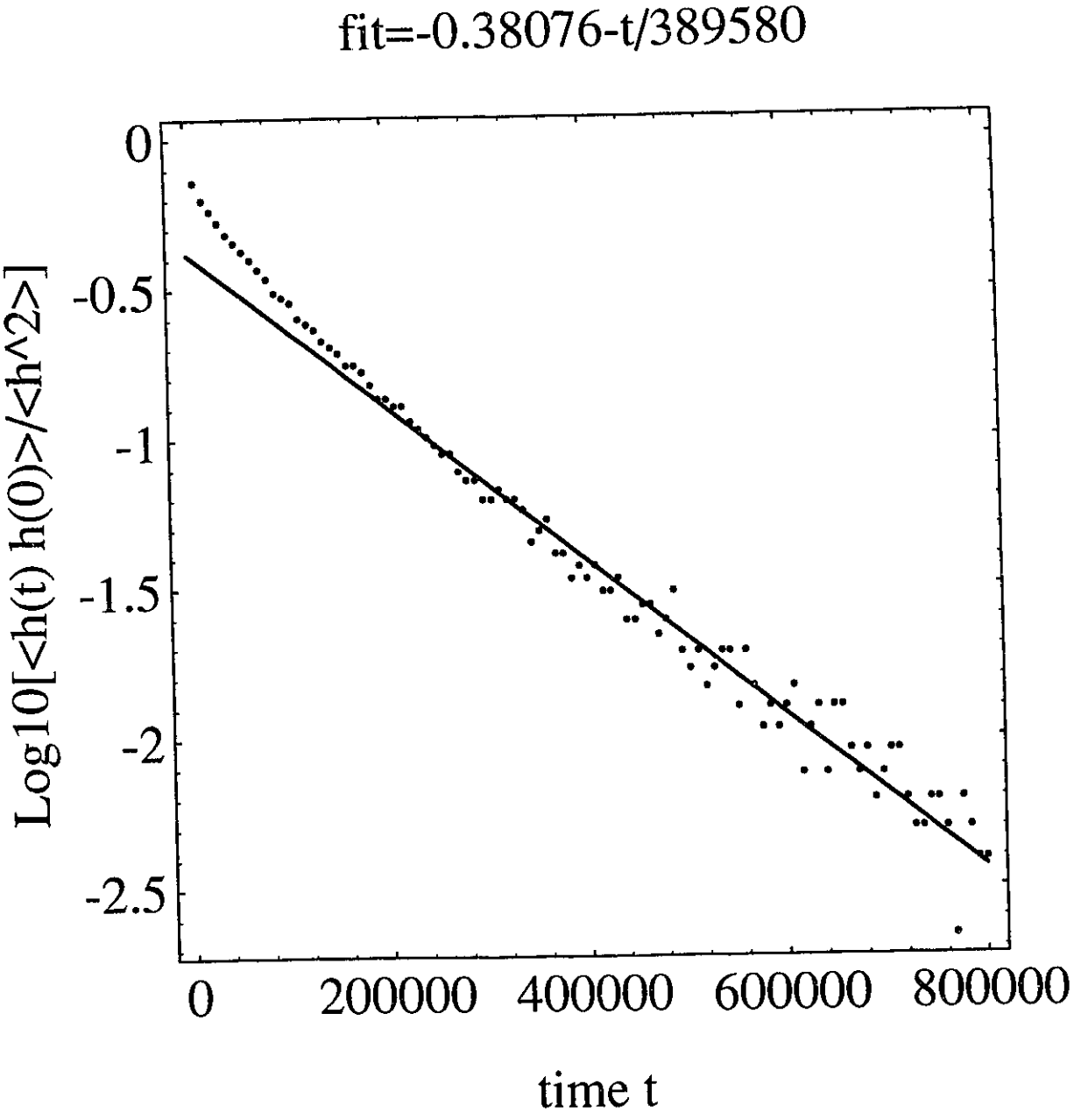

Figure 11. Semi-log plot of log[$\langle \mathbf{h(t)} \cdot \mathbf{h(0)}/h^2(0) \rangle$] vs t for M=20, c=0.9.

vs time t for M=20, c=0.8. It is clear from this plot that there are three distinct regimes here. For early and late times, we see that $\mathbf{R}^2(t) \sim t$. The diffusion coefficient is obtained from the intercept of the fit that describes late time diffusion since the early times are characterized by small displacements between two obstacles. Figure 11 shows a typical plot of $\log[\langle \mathbf{h}(t) \cdot \mathbf{h}(0) \rangle]$ against t for M=20, c=0.8. The early times being characterized by numerous relaxation times, one does not observe a straight line. When the time is long enough, however, the decay is linear, i.e. we have a single relaxation time which is called the terminal relaxation time. We thus obtain the value of τ by fitting the linear part of the decay curve with the expression $A - t/\tau$.

2.4 Diffusion Coefficient vs Concentration

Figure 12 shows how the diffusion coefficient D varies with the obstacle concentration c for polymer molecules of size M=5, 8, 10, 15, 20, 30. We remark a clear reduction of the diffusion coefficient D(M,c) when c decreases from 1.0 to about 0.90, and then a marked increase when c decreases from 0.85 to 0. This non-monatomic behaviour is quite surprising since it means that fewer obstacles makes it more difficult for the polymer molecules to diffuse through the system. As far as we now, this unique signature of entropic trapping has never been reported before. The effect is minimal for M=5, but appears to grow in importance with size M after this point. Figure 13 shows how the terminal relaxation time of the end-to-end vector **h** varies with concentration c for the molecules M=10. Clearly, the internal dynamics of the molecules is also affected since the relaxation time goes though a shallow minimum around c=0.80. The M=10 molecules relax faster with a concentration c=0.80 than with a lower concentration c=0.78. The radius of gyration also goes through a shallow minimum at this point (see Fig. 14).

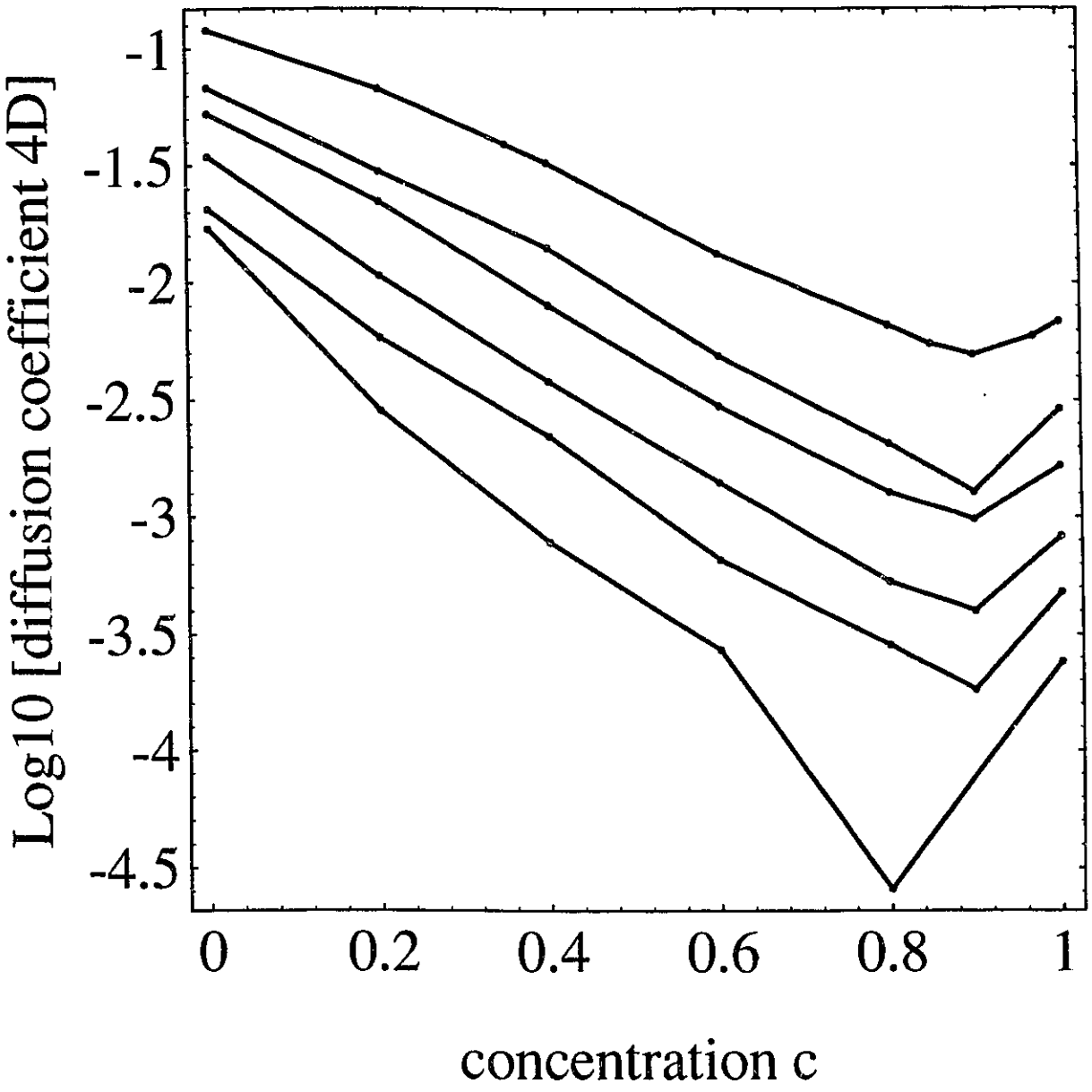

Figure 12. Semi-log plot of the diffusion coefficient D vs obstacle concentration c for polymer molecules of length (from top to bottom) M=5, 8, 10, 15, 20, 30. A clear minimum is observed when c≈0.9. This non-monotonic behaviour means that fewer obstacles makes it more difficult to the polymer molecules to diffuse through the system and represents a strong evidence that entropic trapping occurs.

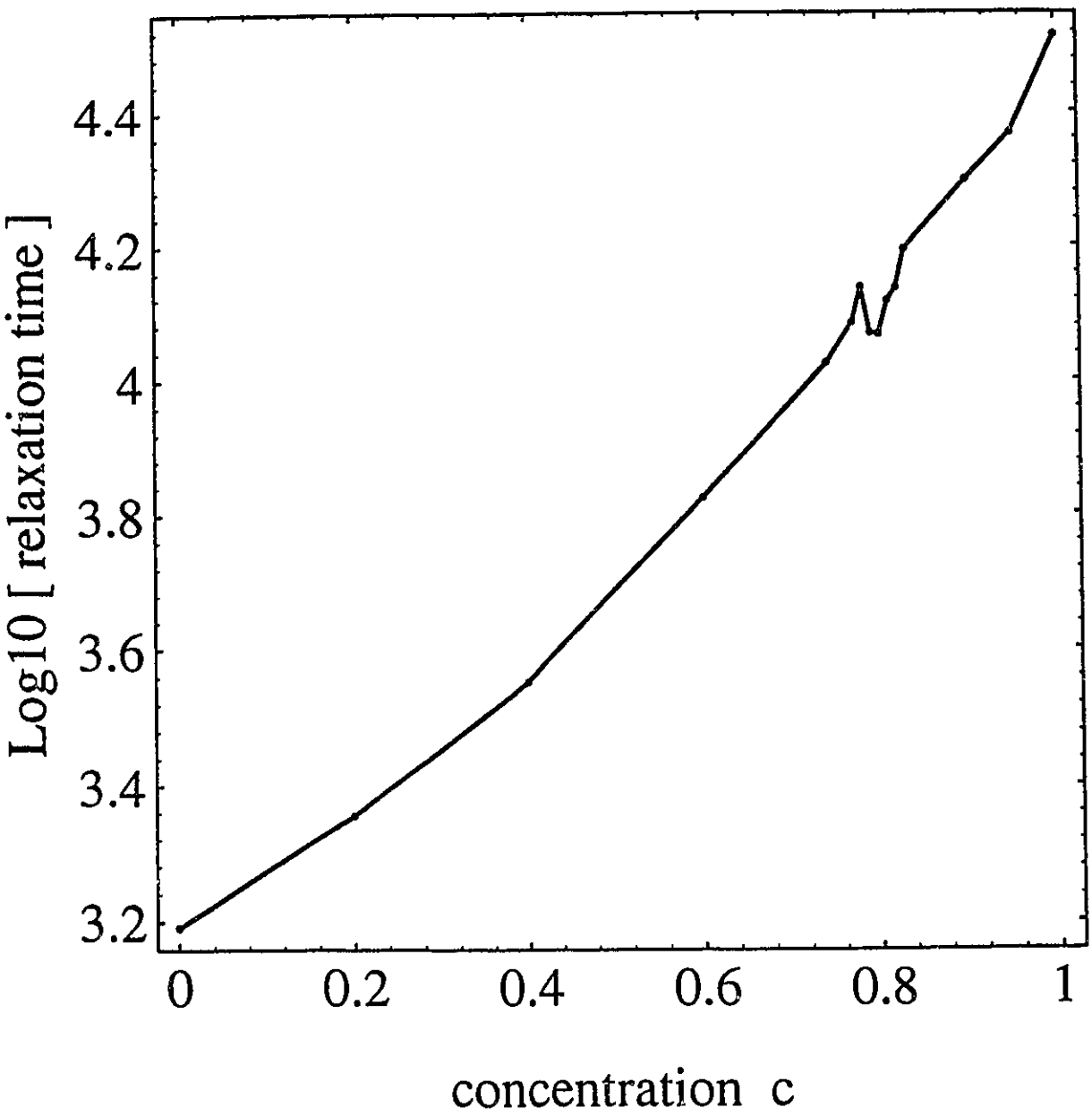

Figure 13. Terminal relaxation time τ of the end-to-end vector h vs concentration c for polymer molecules of length M=10. Again, the non-monotonic behaviour of τ is a strong indication that the disorder in the lattice of obstacle lead to strong polymer localisation for c≈0.80.

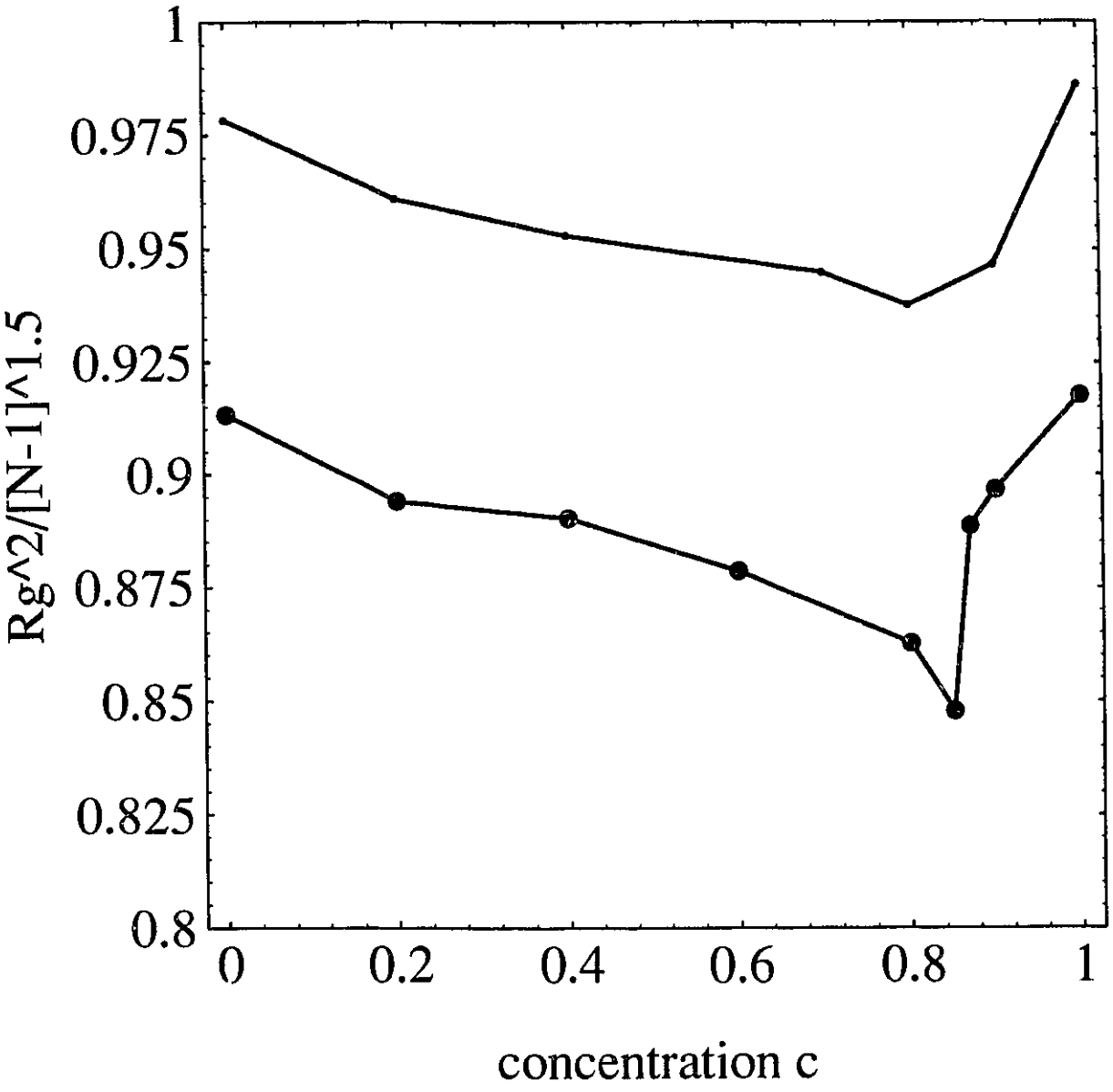

Figure 14. The mean square radius of gyration Rg^2 vs concentration c for polymer molecules of length (form top to botton) M=10, 20.

2.5 Diffusion Coefficient vs Molecular Size

Entropic trapping has been traditionally studied in terms of the dependence of the diffusion coefficient D(M,c) upon molecular size. The Rouse model, which is expected to be valid in the small c limit, predicts $D \sim M^{-1}$, while in the Reptation limit (c=1) we expect $D \sim M^{-2}$. Figure 15 shows how the exponent α, defined by $D \sim M^{-\alpha}$, varies with concentration c. We observe that the exponent increases beyond the value 2 when the concentration decreases from c=1.0 to c≈0.4 (this increase is characteristic of entropic trapping), and then decreases to a value of 1 for c=0, as it should. Figure 16 shows how we get seven values of α by fitting our diffusion data with the relation $D \sim M^{-\alpha}$ for c=0, 0.2, 0.4, 0.6, 0.8, 0.9 and 1.0.

Figure 12-15 thus showed the existence of an intermediate regime, between the Rouse and Reptation limits, where the diffusion coefficient is lower and more molecular size-dependent that expected. Moreover, this regime is characterized by somewhat fast-relaxing compact conformations. Our results also indicate that this intermediate regime disappears (the exponent $\alpha<2$) when the concentration of obstacle decreases below about 40%. Very small molecules do not seem to be affected by this intermediate regime.

2.6 Density Plots

In order to investigate the nature of the regime where the diffusion properties of the polymer cannot be explained by Reptation or Rouse dynamics, we computed the number of times the 4 middle monomers (we do not count the end monomers since the latter can visit areas of the system that the molecule as a whole does not actually visit) of the polymer chains visited

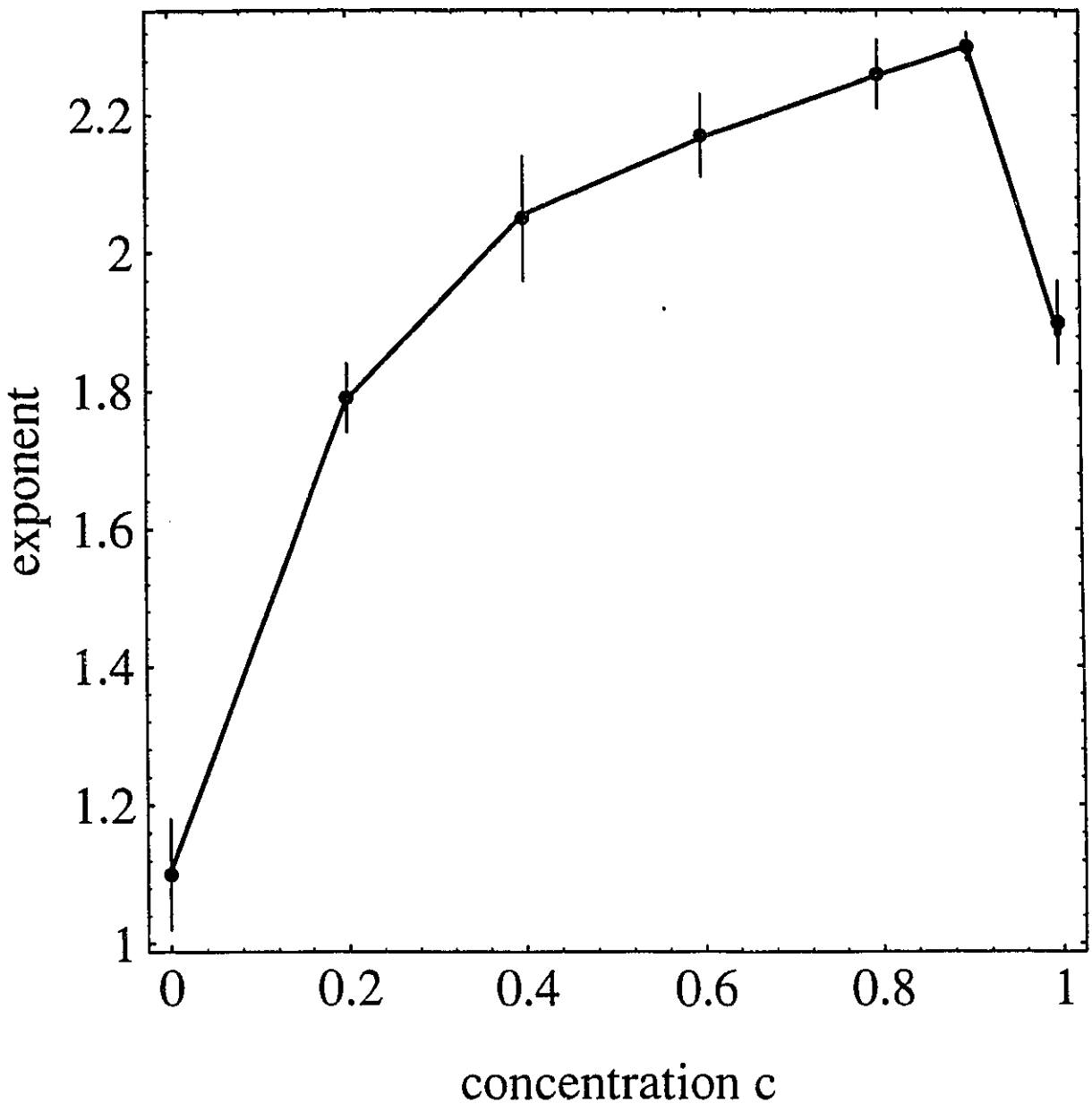

Figure 15. Exponent α vs concentration. The exponent was obtained from the fit of the diffusion constant to the form $D \sim M^{-\alpha}$. The Rouse model, which is expected to be valid in the small c limit, predicts $D \sim M^{-1}$, while in the reptation limit (c=1) we expect $D \sim M^{-2}$. The exponent increases beyond 2 when the concentration decreases from c=1.0 to c=0.4, and then decreases towards a value of 1 for c=0.

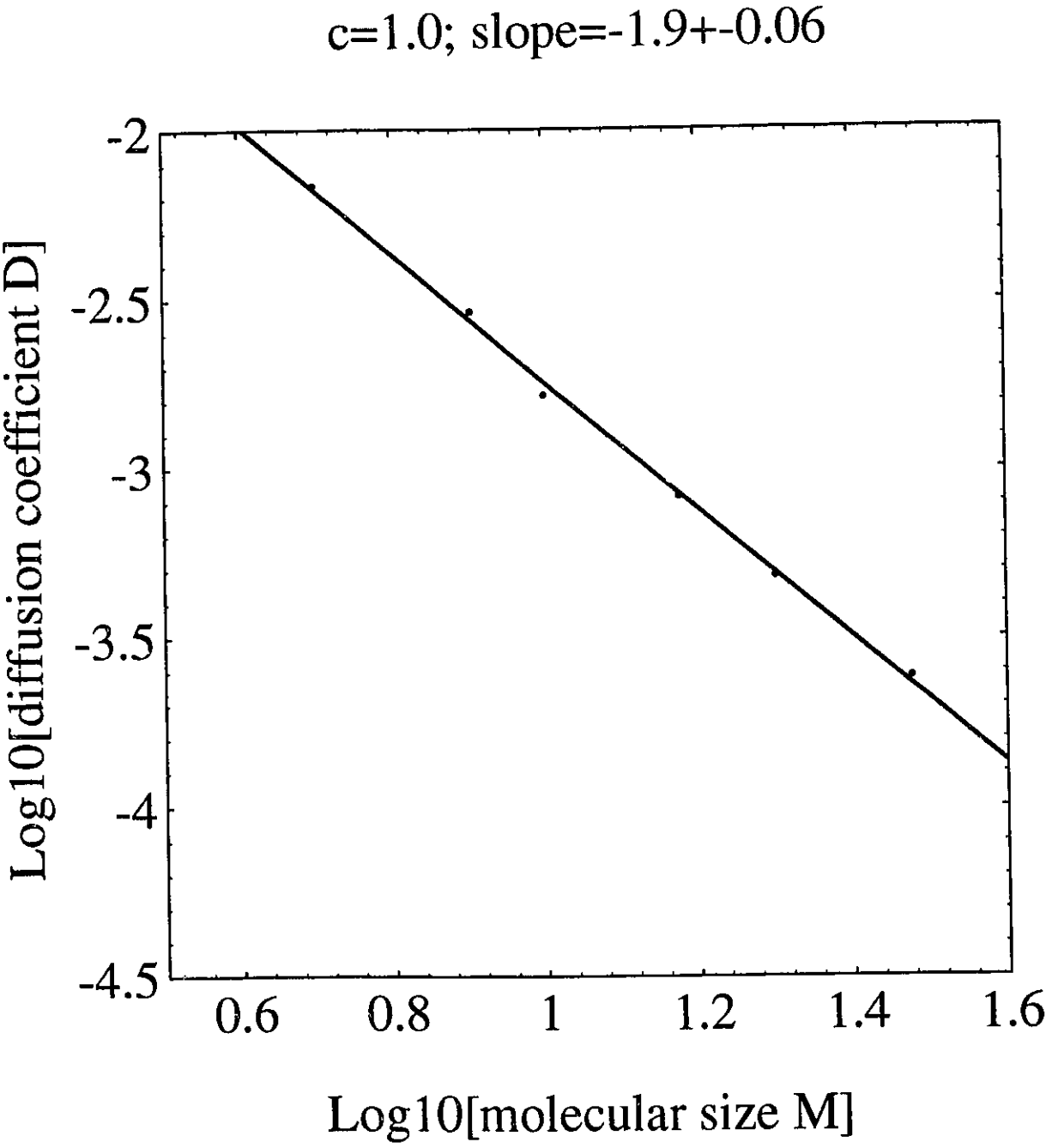

Figure 16. Log-log plot of the diffusion coefficient D vs M for various c. (a) c=1.0.

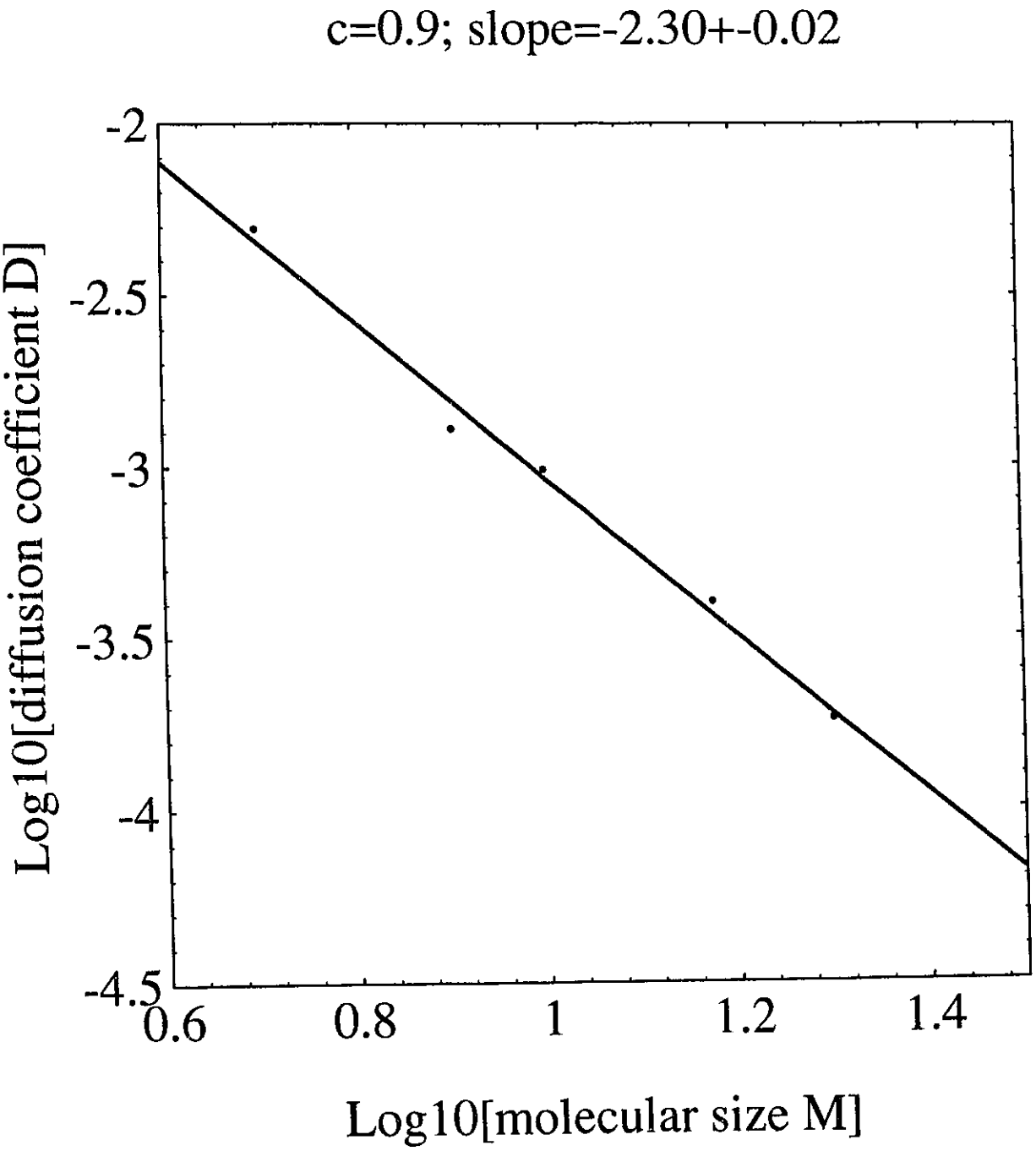
c=0.9; slope=-2.30+-0.02
-2
-2.5
-3
-3.5
-4
-4.5
0.6
0.8
1
1.2
1.4
Log10[diffusion coefficient D]
Log10[molecular size M]

(b) c=0.9

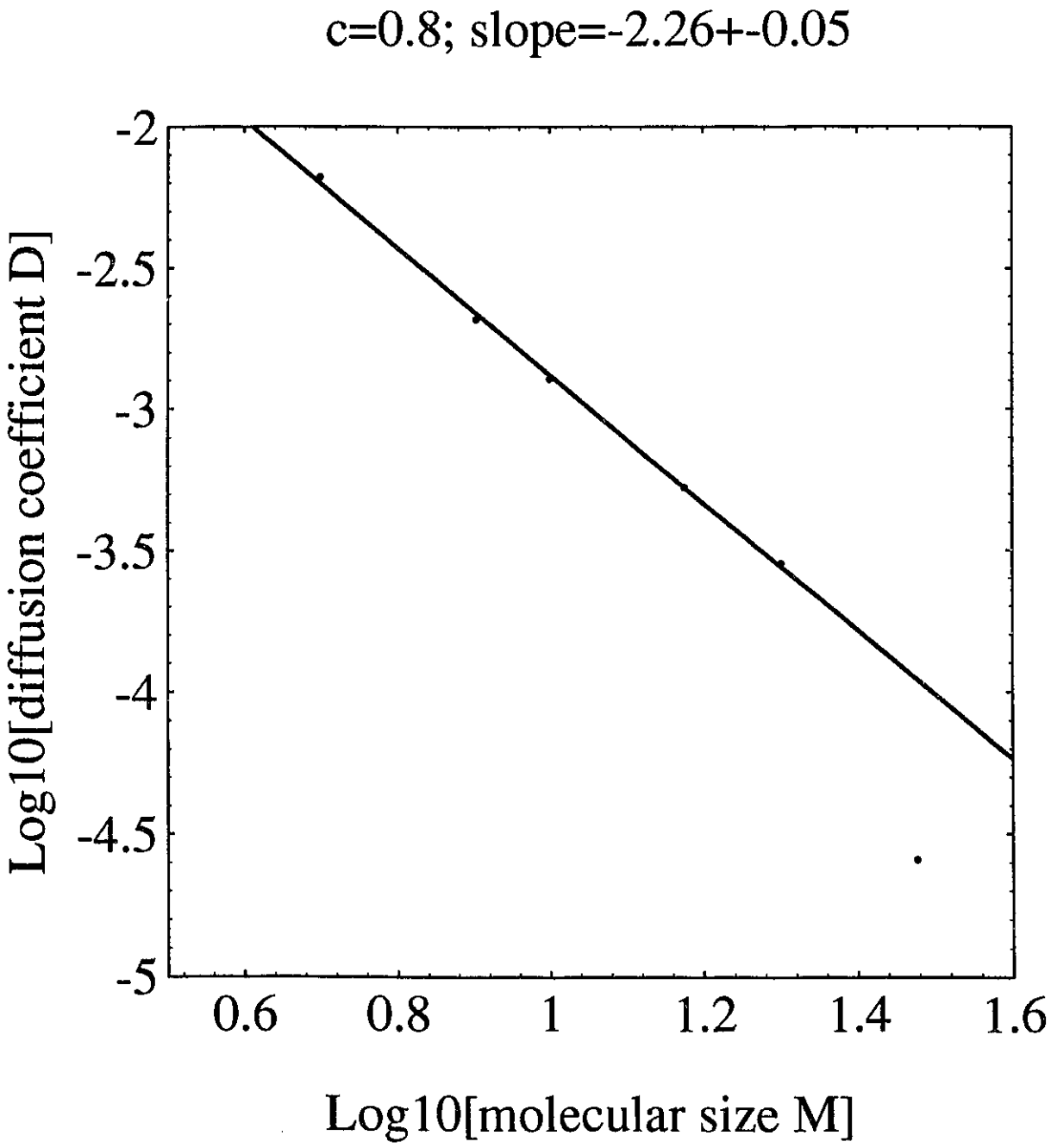

(c) c=0.8; the data point for M=30 was not used.

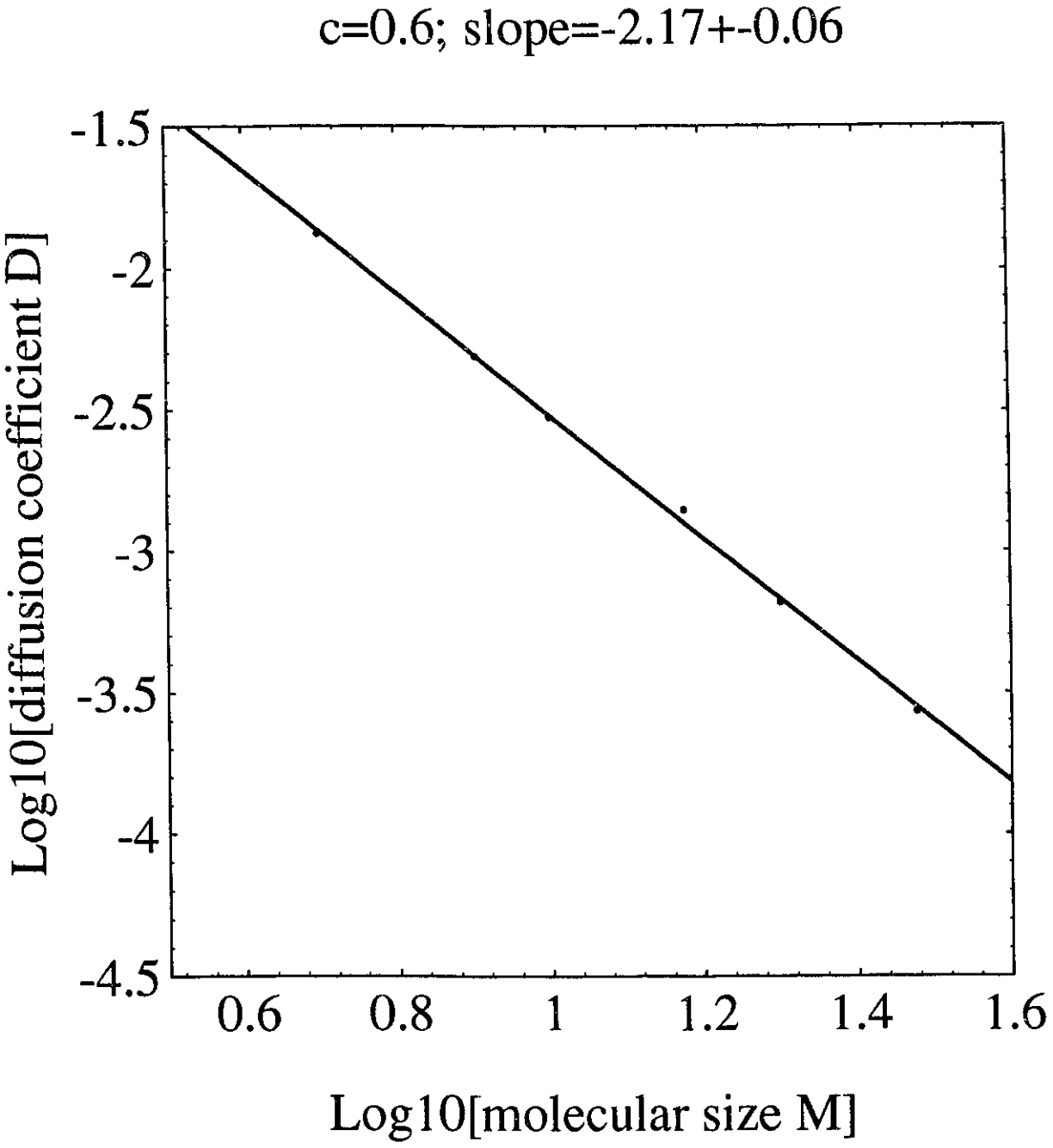
c=0.6; slope=-2.17+-0.06
-1.5
-2
-2.5
-3
-3.5
-4
-4.5
Log10[diffusion coefficient D]
0.6
0.8
1
1.2
1.4
1.6
Log10[molecular size M]

(d) c=0.6

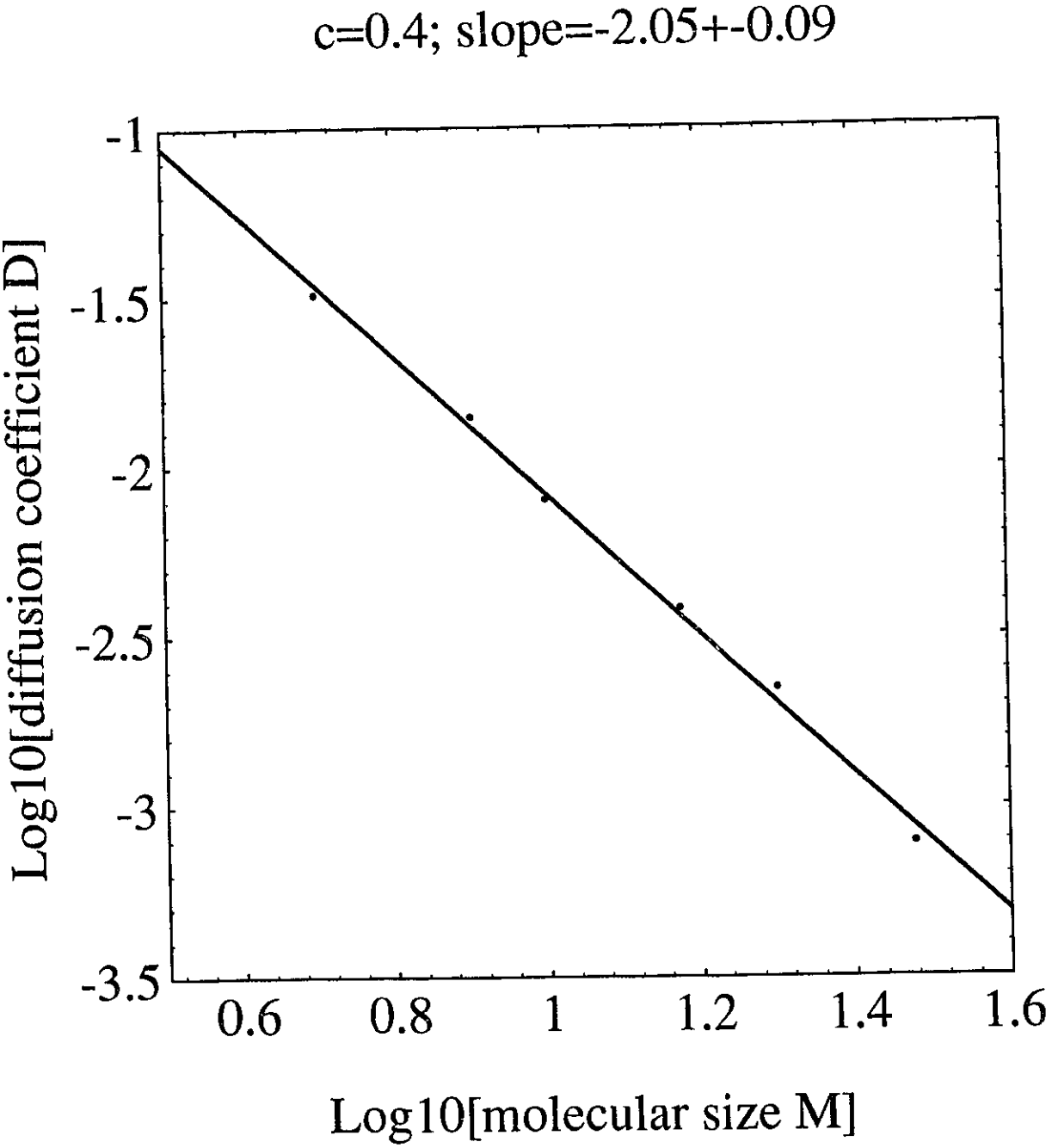
c=0.4; slope=-2.05+-0.09
Log10[diffusion coefficient D]
-1
-1.5
-2
-2.5
-3
-3.5
0.6
0.8
1
1.2
1.4
1.6
Log10[molecular size M]

(e) c=0.4

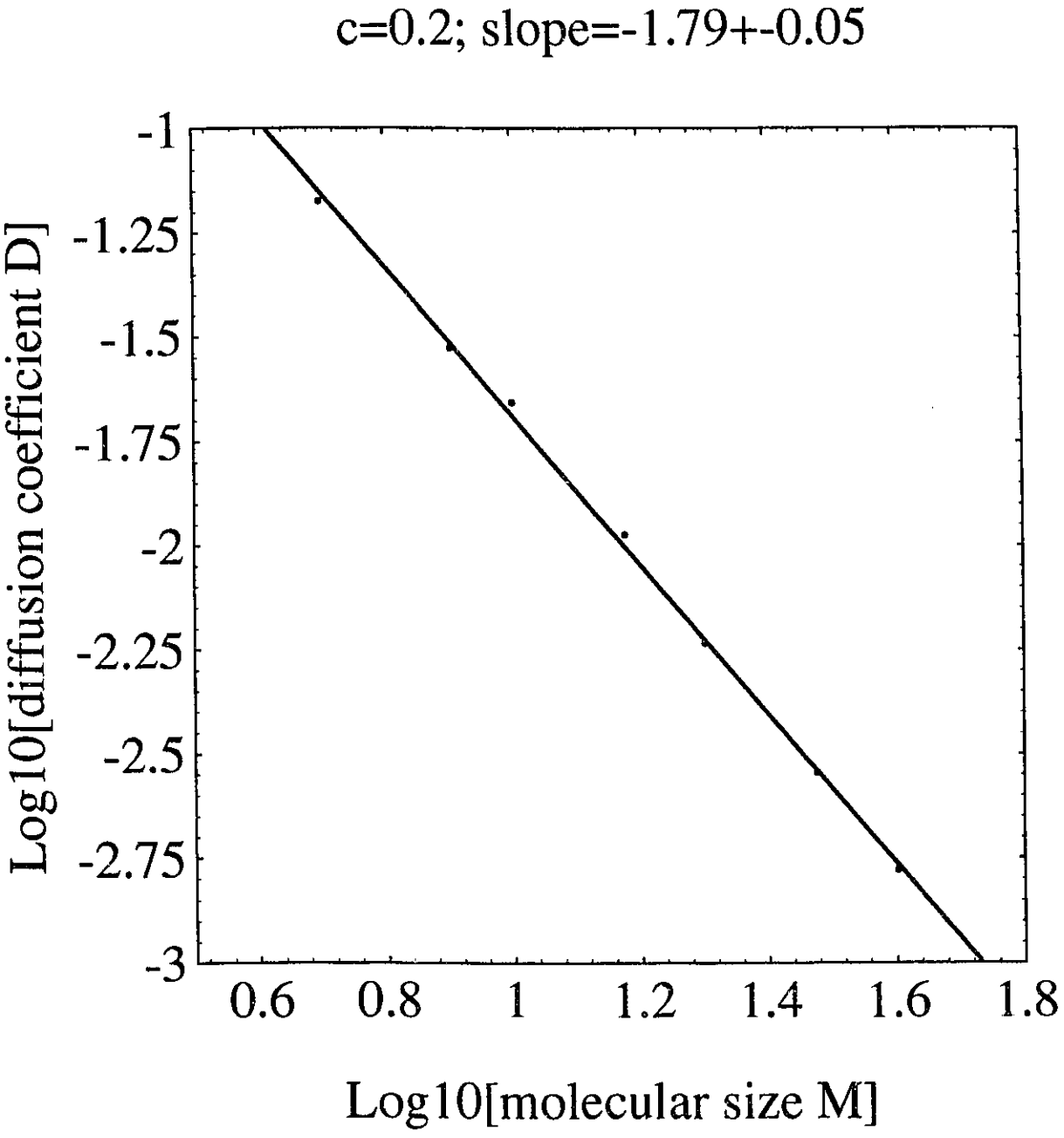
c=0.2; slope=-1.79+-0.05
Log10[diffusion coefficient D]
-1
-1.25
-1.5
-1.75
-2
-2.25
-2.5
-2.75
-3
0.6
0.8
1
1.2
1.4
1.6
1.8
Log10[molecular size M]

(f) c=0.2

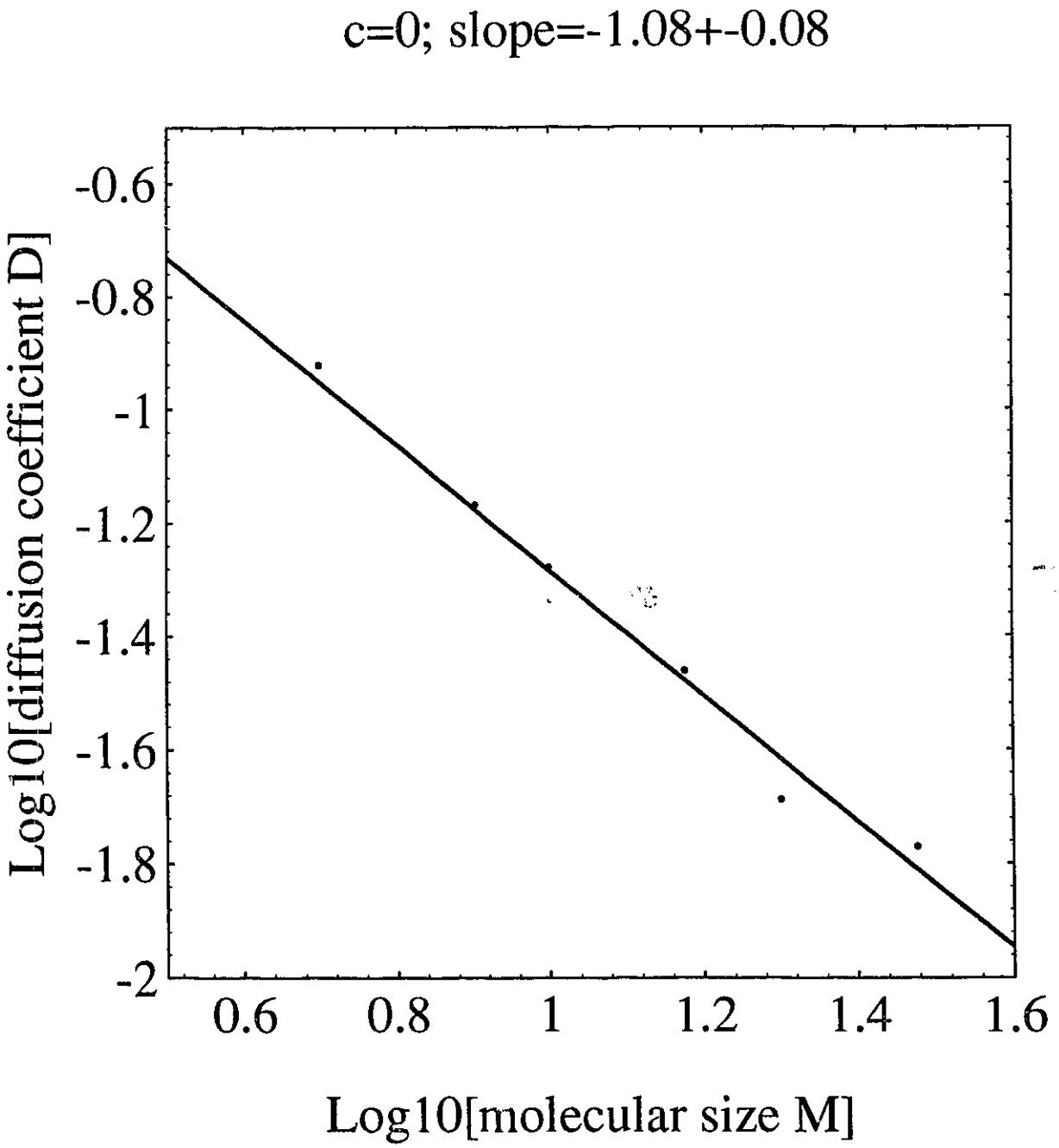
c=0; slope=-1.08+-0.08
Log10[diffusion coefficient D]
-0.6
-0.8
-1
-1.2
-1.4
-1.6
-1.8
-2
0.6
0.8
1
1.2
1.4
1.6
Log10[molecular size M]

(g) c=0

each site in a reduced 96×96 lattice. Figure 17 presents density plots of the lattice with the darker areas representing the sites which have been visited more often. The small white squares are the location of the obstacles. Six different cases are shown. When c=1 the density is uniform, as expected. When c=0.95, the chain is in the trapping regime although only a small fraction of the obstacles have been removed. However, when c=0.90, the chain clearly spends most of its time in large but isolated "pores" where many contiguous obstacles have been removed. The entropy of the molecules being larger in such pores, the latter act as "entropic" traps. The migration between each pore is through reptation since the concentration is near unity between pores. For a more dilute system ($c \leq 0.4$), the obstacles cease to form a percolation cluster and the pores are connected to form wide passages through the entire system. Finally, when the concentration is very small, the obstacles play a minor role and one recovers Rouse dynamics without any entropic trapping. These results are in good agreement with the quantitative results presented before and explain why the entropic trapping regime disappears for $c<40\%$: this critical concentration simply represents the percolation limit of the underlying lattice of obstacles for the chosen geometry.

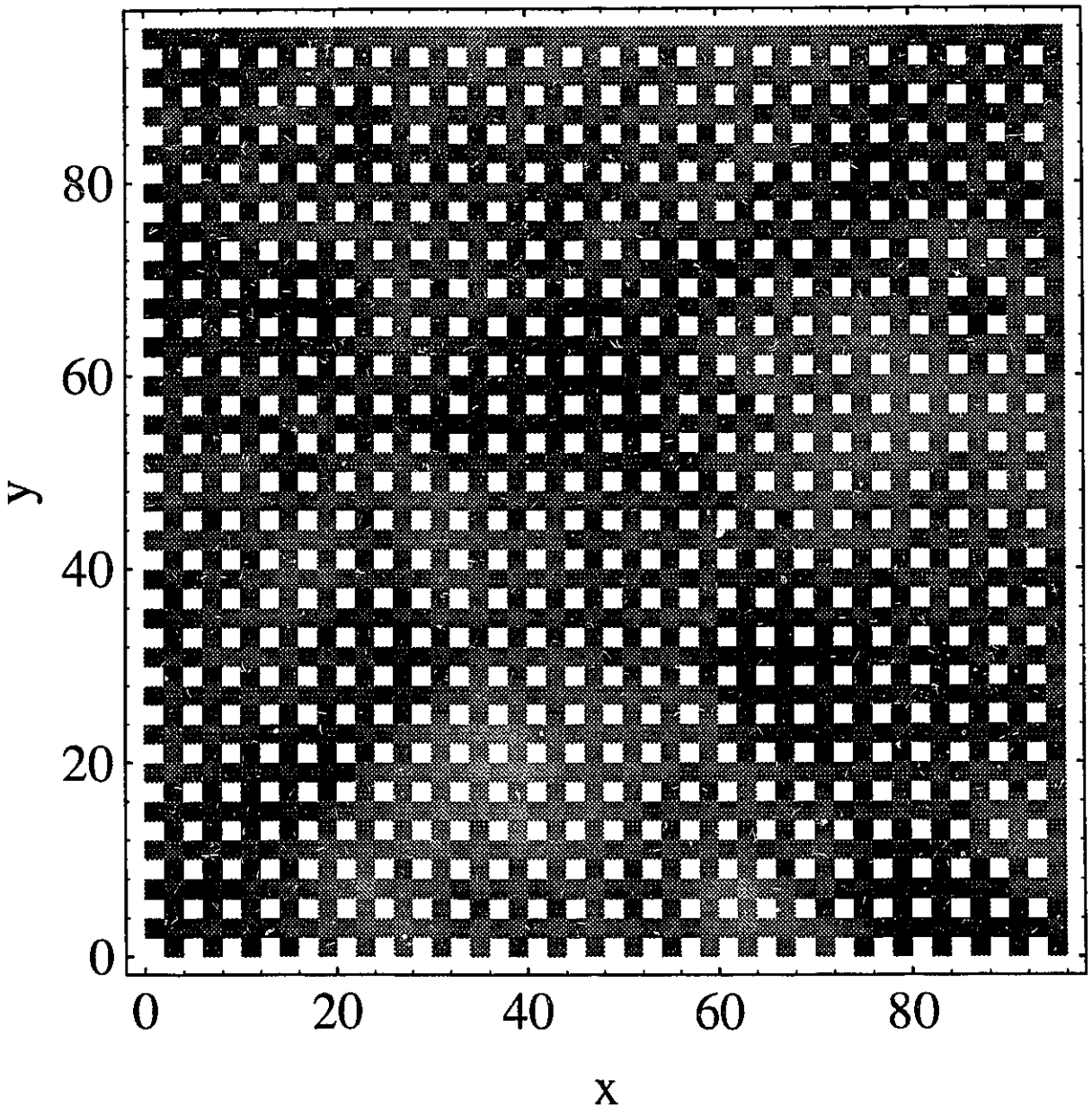

Figure 17. Density plots showing the number of times the (4) middle monomers of the M=10 polymer molecules visited the different sites of a 96 X 96 lattice (with periodic boundary conditions). The darker areas have been visited more often. The small white squares are centered at the location of the obstacles. (a) c=1: the density is uniform since all the obstacles are present.

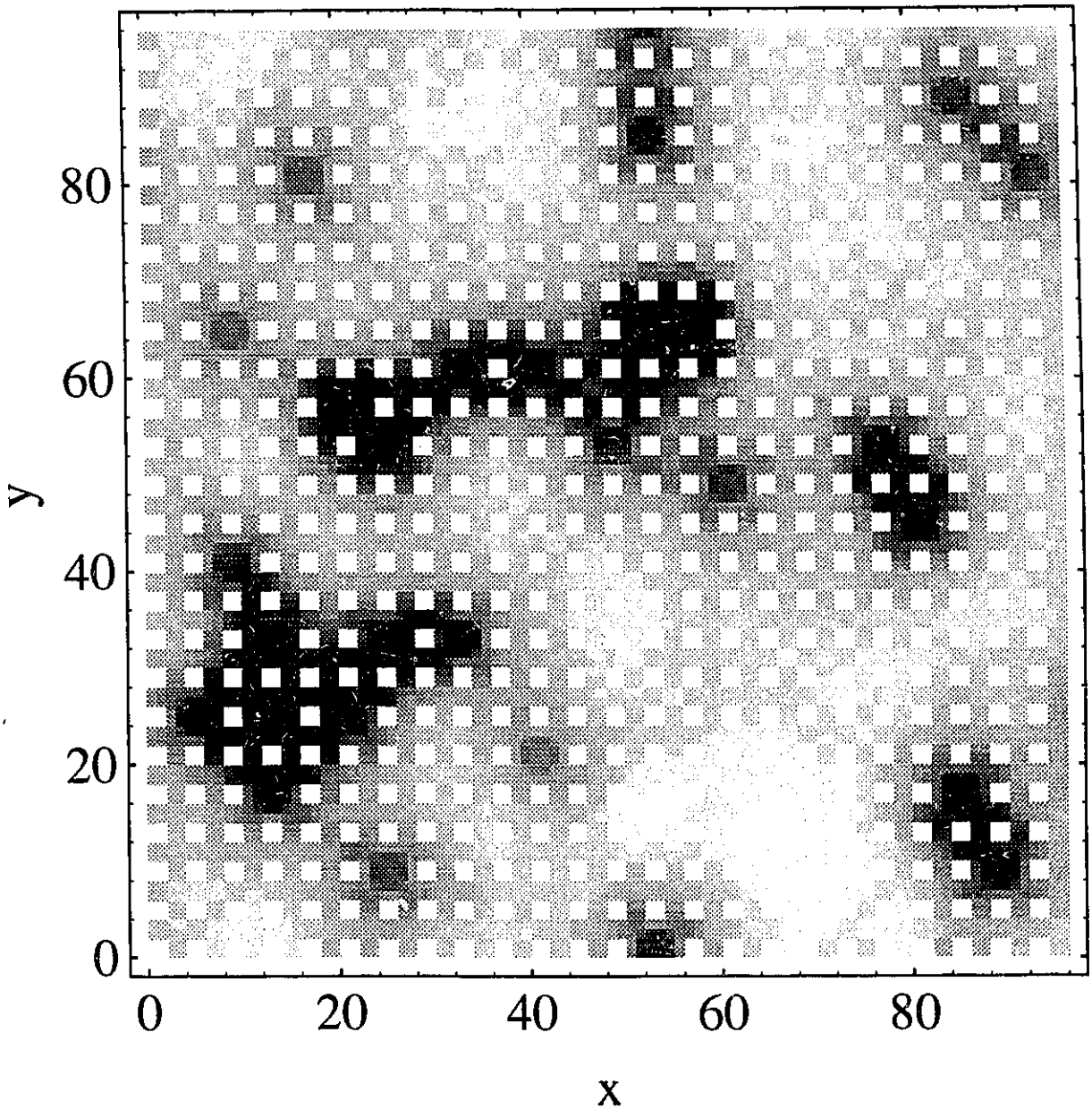

(b) c=0.95: the chain shows to be in trapping regime although small fraction obstacles are removed.

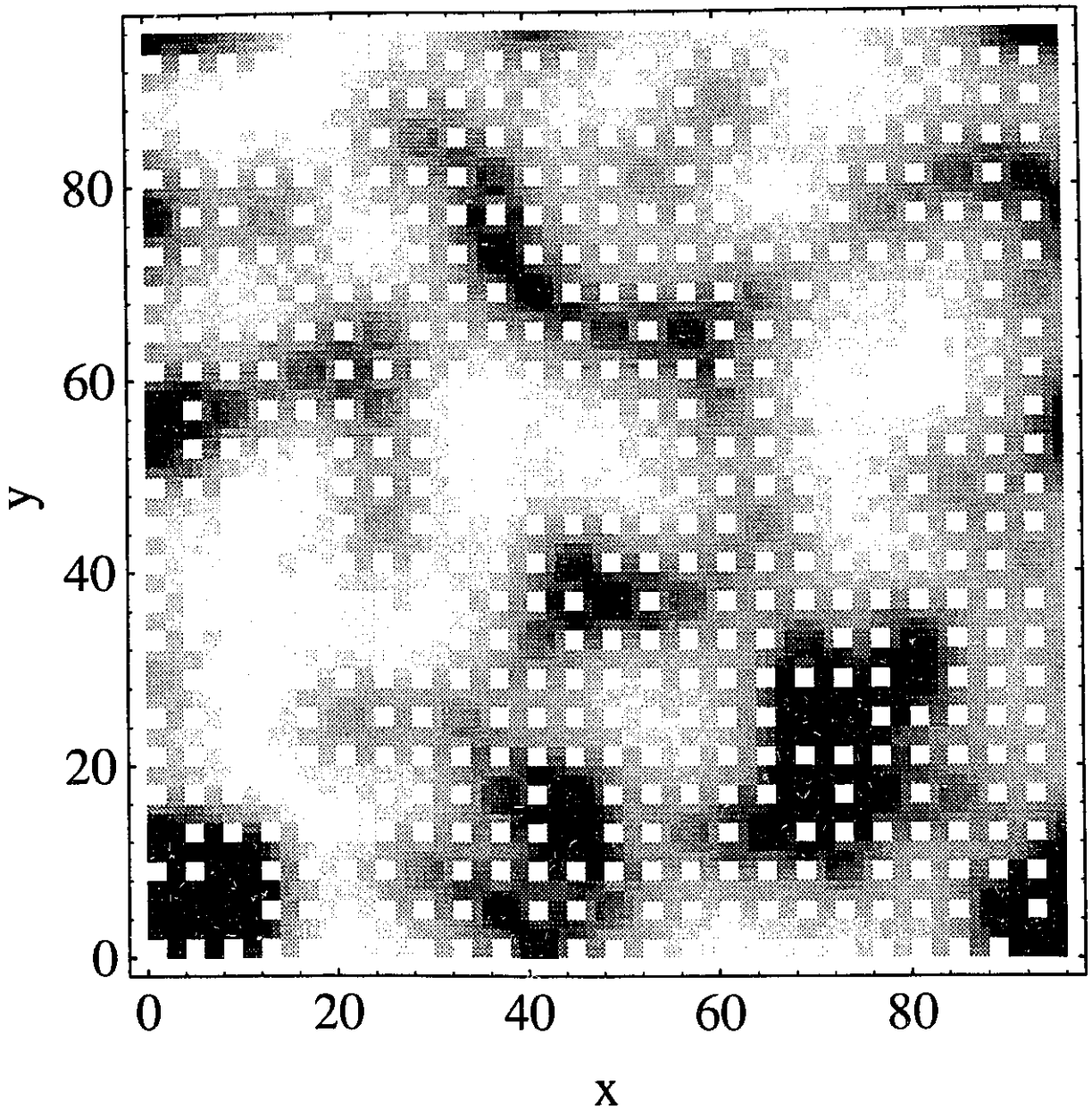

(c) c=0.9: the chain clearly spends most of its time in large but isolate "pores".

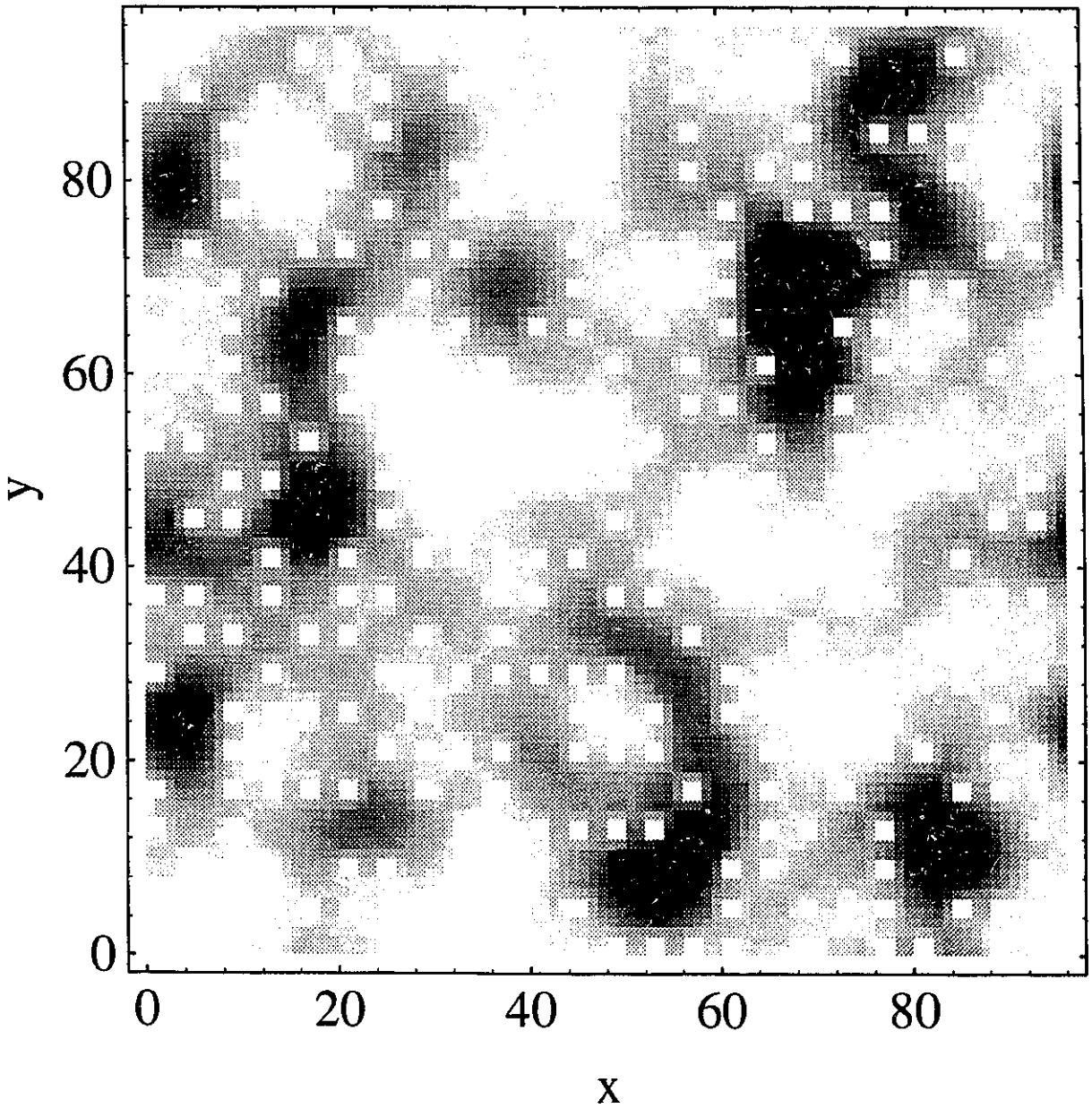

(d) c=0.6: the pores are more connected and the chain bexomes less localized.

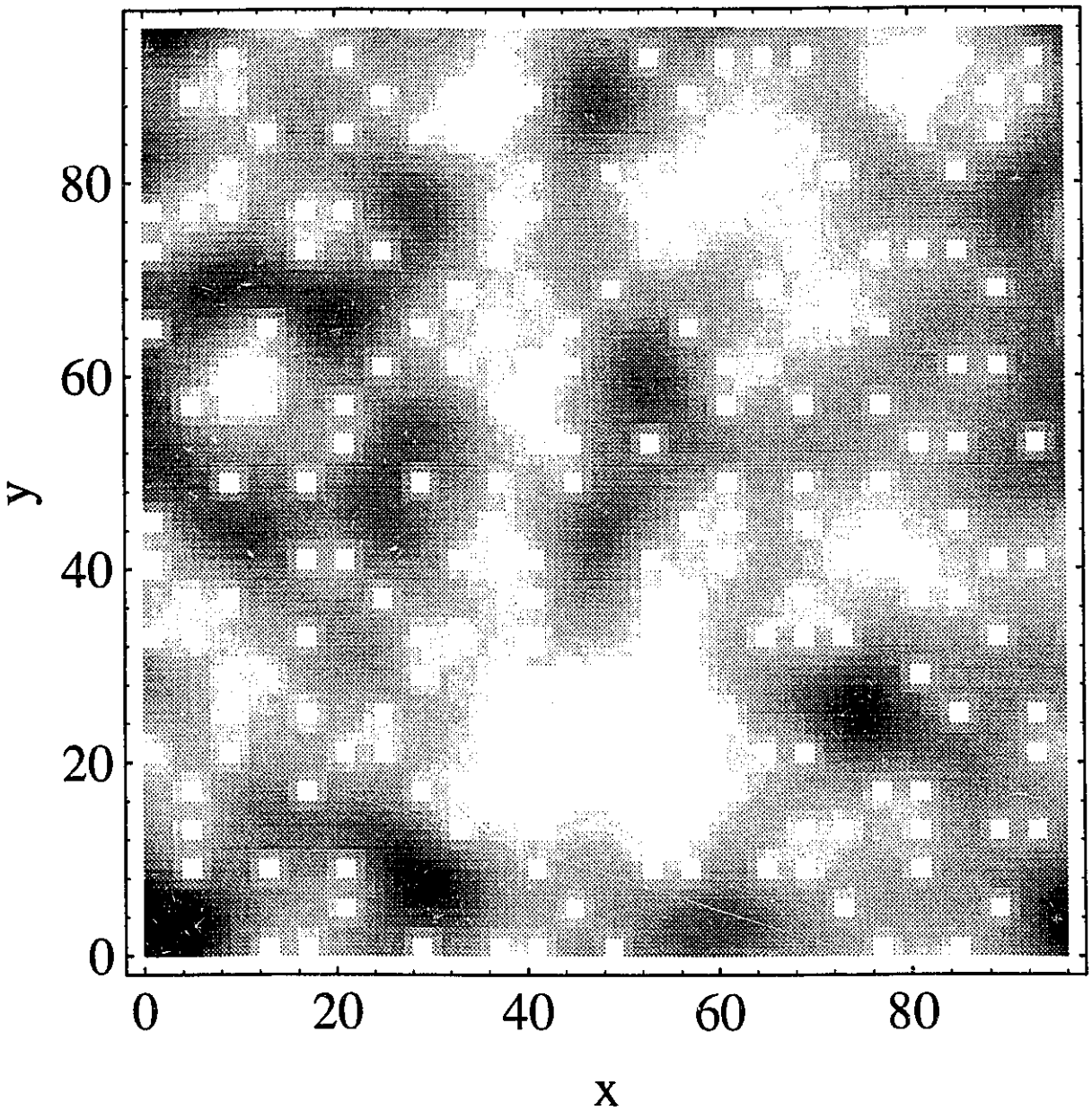

(e) c=0.4: the pores are connected by wide passages that form a percolating path through the entire system.

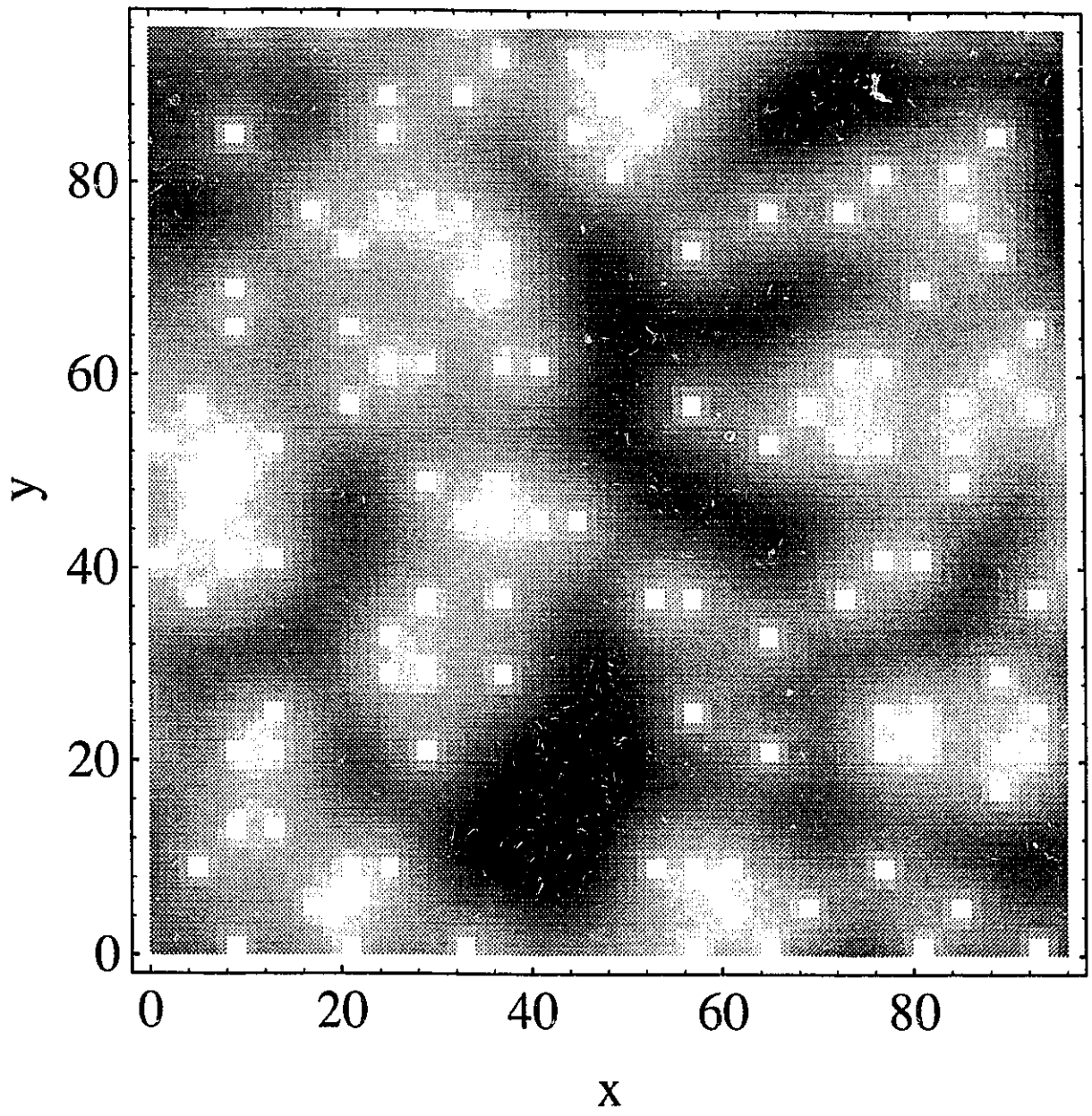

(f) c=0.2: the obstacles now play a somewhat minor role and one soon recovers Rouse Dynamics.

Chapter 3

Conclusion

Our simulation results indicate that the diffusion constant of a macromolecule is not necessarily a monotonically decreasing function of the density of the medium. This new and unexpected prediction is directly related to the entropic properties of polymers in random environments, and to the nature of the randomness (and the percolation limit) of this environment.

Using Monte Carlo simulations, Saxton[34] found that the diffusion coefficient of spherical particles is independent of the size of the particles for certain fractal obstacles. The fractal obstacles were constructed using a CCA[35] (cluster-cluster aggregation) model. In CCA models, clusters carry out random walks on a lattice and adhere rigidly and irreversibly to each other upon contact. The process continues until only one cluster is left. It would be interesting to study the motion of polymers in such systems.

Besides this simulation result, a number of situations where the electrophoretic mobility of polyelectrolytes shows strange behaviours have been reported. Mayer et al[31]. and Arvanitidou et al[29,37]. have observed cases where anomalous migration might be due to the type of entropic trapping described in this thesis. However, cases where the mobility is a non-monotonic function of gel concentration still have to be observed.

Clearly, the diffusion properties of macromolecules are influenced by the details of the architecture of the environment and of the molecule itself[30]. This means that one must be careful when analyzing experimental data since non-trivial results as those presented here can happen.

Also, any mean-field like theoretical study of randomness is useless since the detailed nature of the randomness is important. The system studied here could also be studied (experimentally or theoretically) using the "2D arrays of posts" of Volkmuth and Austin[38], which is a microlithographically constructed 2D rectangular array of cylindrical posts. Note that the tracer chain must be sufficiently flexible to approximate RW behavior, and the radius of gyration of the chain must be comparable to the radius of the "mean pore" in the medium.

Muthukumar et al[26-28] have previously studied the diffusion of a polymer chain in random media, but did not observe the non-monotonic dependence of the diffusion constant upon concentration. The reason is that the (percolation-like) random environment used by Muthukumar and Baumgartner was different from what we use. Presumably, a more realistic gel would be more like the structures formed by CCA, or similar algorithms. It is not inconceivable that one might have other types of random environments where the diffusion constant might become a non-monotonically decreasing function of the molecular size of the polymer.

Finally, our results also indicate that very little randomness is necessary to kill reptation. In fact, density plots show that c=0.97 is already in the trapping regime (see figure 17b). At this time, we are studying quantitatively the stability of reptation vs the degree of randomness in our system. It appears that reptation is an intrinsically unstable process in a randomly frozen environment, i.e. that the chains quickly get entropically trapped in large pores and this dominates the long-term diffusion. The situation for very large molecules, which can span the distance between two large pores, should be most interesting since, in principle, these molecules should eventually reptate.

References

(1) Chrambach, A. ; Rodbard, D. *Science* **1971**, *170*, 440.

(2) Guo, X.-H. ; Chen, S. -H. *Phys. Rev. Lett.*. **1990**, *64*, 2579.

(3) Smisek, D. L. ; Hoagland, K. A. *Macromolecules* **1989**, 22, 2270.

(4) Lumpkin, O. J. ; Déjardin, P. ; Zimm, B. H. *Biopolymers* **1985**, *24*, 1573.

(5) Slater, G. W. ; Rousseau, J. ; Noolandi, J. *Biopolymers* **1987**, *26*, 863.

(6) Smith, S. B. ; Aldridge, P. K. ; Callis, J. B. *Science* **1989**, *243*, 203.

(7) Schwartz, D. C. ; Koval, M. *Nature* **1989**, *338*, 520.

(8) Schwartz, D. C. ; Cantor, C. R. *Cell* **1984**, *37*, 67.

(9) Platt, K. J. ; Holzwarth, G. *Phys. Rev. A* **1989**, *40*, 7292.

(10) Slater, G. W. ; Noolandi, J. ; Eisenberg, A. *Macromolecules* **1991**, *24*, 6715.

(11) Slater, G. W. ; Noolandi, J. *Macromolecules* **1986**, *19*, 2356.

(12) Lumpkin, O. ; Levene, S. D. ; Zimm, B. H. *Phys. Rev.* **1989**, *39*, 6557.

(13) Slater, G. W. *Journal de Physique II* **1992**, *2*, 1149.

(14) Ulanovsky, L. ; Drouin, G. ; Gilbert, W. *Nature* **1990**, *190*, 343.

(15) Viovy, J. L. ; Défontaines, A. D. *In Pulsed-Field Gel Electrophoresis, Protocol, Methods and Theories* 1992, p 403-450, Humana Press: Totowa, New Jersey.

(16) de Gennes, P. -G. *J. Chem. Phys.* **1971**, *55*, 572.

(17) Doi, M. ; Edwards, S. F. *J. Chem. Soc. , Faraday Trans. 2* **1978**, *74*, 1789.

(18) Smith, S. B. ; Aldridge, P. K. ; Callis, J. B. *Science* **1989**, *243*, 203.

(19) Rudnick, J. ; Gaspari, G. ; *Science* **1987**, *237*, 384.

(20) Deutsch, J. M. ; Madden, T. L. *J. Chem. Phys.* **1989**, *90*, 2476.

(21) Noolandi, J. ; Rousseau, J. ; Slater, G. W. ; Turmel, C. ; Lalande, M. *Phys. Rev. Lett.* **1987**, *58*, 2428.

(22) Marshall, W. ; Lovesey, S. W. *Theory of Thermal Neutron scattering* **1987**, Oxford Univ Press.

(23) Chu, B. *Laser Light Scattering* **1974**, Academic Press, New York.

(24) Berne, B J. ; Pecora, R. *Dynamic Light Scattering* **1976**, Wiley, New york.

(25) Doi, M. ; Edward, S. F. *The Theory of Polymer Dynamics* **1986**, Clarendon: Oxford.

(26) Muthukumar, M. ; Baumgartner, A. *Macromolecules* **1989**, *22*, 1937.

(27) Muthukumar, M. ; Baumgartner, A. *Macromolecules* **1989**, *22*, 1941.

(28) Muthukumar, M. *J. Non-Cryst. Solids* **1991**, *131-133*, 654.

(29) Arvanitidou, E. ; Hoagland, D. *Phys. Rev. Lett.* **1991**, *67*, 1464.

(30) Hoagland, D. ; Muthukumar, M. *Macromolecules* **1992**, *25*, 6696.

(31) Mayer, P. ; Slater, G. W. ; Drouin, G. *Applied and Theoretical Electrophoresis* **1993**, *3*, 147.

(32) Carmesin, I. ; Kremer, K. *Macromolecules* **1988**, *21*, 2819.

(33) Duke, T. A. *J. Chem. Phys.* **1990**, *93*, 9049.

(34) Saxton, M. J. *Biophysical J.* **1993**, *61*, 119.

(35) Saxton, M. J. *Biophysical J.* **1993**, *64*, 1053.

(36) Noolandi, J. ; Rousseau, J. ; Slater, G .W.; Turmel, C.; Lalande, M. *Phys. Rev. Lett.* **1987**, *58*, 2428.

(37) Arvanitidou, E. ; Hoagland, D. ; Smisek, D. *Biopolymers* **1991**, *31*, 435.

(38) Volkmuth, W. D. ; Austin, R. H. *Nature* **1992**, *358*, 600.